Integrated Ocean Drilling Program
Expedition 343/343T Preliminary Report

Japan Trench Fast Drilling Project (JFAST)

1 April–24 May 2012 and 5–19 July 2012

Frederick M. Chester, James J. Mori, Sean Toczko,
Nobu Eguchi, and the Expedition 343/343T Scientists

Published by
Integrated Ocean Drilling Program Management International, Inc.,
for the Integrated Ocean Drilling Program

Publisher's notes

Citation:
Chester, F.M., Mori, J.J., Toczko, S., Eguchi, N., and the Expedition 343/343T Scientists, 2012. Japan Trench Fast Drilling Project (JFAST). *IODP Prel. Rept.,* 343/343T. doi:10.2204/iodp.pr.343343T.2012

Distribution:
Electronic copies of this series may be obtained from the Integrated Ocean Drilling Program (IODP) Scientific Publications homepage on the World Wide Web at **www.iodp.org/scientific-publications/.**

This publication was prepared by the Japanese Implementing Organization, Center for Deep Earth Exploration (CDEX) at the Japan Agency for Marine-Earth Science and Technology (JAMSTEC), as an account of work performed under the international Integrated Ocean Drilling Program (IODP), which is managed by IODP Management International (IODP-MI), Inc. Funding for the program is provided by the following agencies:

National Science Foundation (NSF), United States

Ministry of Education, Culture, Sports, Science and Technology (MEXT), Japan

European Consortium for Ocean Research Drilling (ECORD)

Ministry of Science and Technology (MOST), People's Republic of China

Korea Institute of Geoscience and Mineral Resources (KIGAM)

Australian Research Council (ARC) and GNS Science (New Zealand), Australian/New Zealand Consortium

Ministry of Earth Sciences (MoES), India

Disclaimer

October 2012

Expedition 343/343T participants

Expedition 343 scientists

James J. Mori
Co-Chief Scientist
Earthquake Hazards Division
Disaster Prevention Research Institute
Kyoto University
Gokasho, Uji
Kyoto 611-0011
Japan
mori@eqh.dpri.kyoto-u.ac.jp

Frederick M. Chester
Co-Chief Scientist
Center for Tectonophysics
Department of Geology and Geophysics
Texas A&M University
College Station TX 77843-3115
USA
chesterf@tamu.edu

Nobuhisa Eguchi
Expedition Project Manager/Staff Scientist
Center for Deep Earth Exploration
Japan Agency for Marine-Earth Science and Technology
3173-25 Showa-machi, Kanazawa-ku
Yokohama, Kanagawa 236-0001
Japan
neguchi@jamstec.go.jp

Sean Toczko
Expedition Project Manager/Staff Scientist
Center for Deep Earth Exploration
Japan Agency for Marine-Earth Science and Technology
3173-25 Showa-machi, Kanazawa-ku
Yokohama, Kanagawa 236-0001
Japan
sean@jamstec.go.jp

Yukari Kido
Logging Staff Scientist
Center for Deep Earth Exploration
Japan Agency for Marine-Earth Science and Technology
3173-25 Showa-machi, Kanazawa-ku
Yokohama, Kanagawa 236-0001
Japan
Kidoy@jamstec.go.jp

Saneatsu Saito
Associate Logging Staff Scientist
Institute for Research on Earth Evolution (IFREE)
Japan Agency for Marine-Earth Science and Technology
2-15 Natsushima-cho, Yokosuka
Kanagawa 237-0061
Japan
saito@jamstec.go.jp

Yoshinori Sanada
Associate Logging Staff Scientist
Center for Deep Earth Exploration
Japan Agency for Marine-Earth Science and Technology
3173-25 Showa-machi, Kanazawa-ku
Yokohama, Kanagawa 236-0001
Japan
sanada@jamstec.go.jp

Louise Anderson
Logging Scientist
Department of Geology
University of Leicester
University Road
Leicester LE1 7RH
United Kingdom
lma9@le.ac.uk

Jan H. Behrmann
Physical Properties Specialist
GEOMAR
Helmholtz Centre for Ocean Research Kiel
Wischhofstraße 1-3
24148 Kiel
Germany
jbehrmann@geomar.de

Santanu Bose
Structural Geologist
University of Calcutta
Department of Geology
35, Ballygunge Circular Road
Kolkata-700 019
India
bose.santanu@gmail.com

Marianne Conin
Logging Scientist/Physical Properties Specialist
CEREGE
Europôle Méditerranéen de l'Arbois
Avenue Louis Philibert
BP 80
13545 Aix en Provence Cedex 04
France
conin@cdf.u-3mrs.fr

Becky Cook
Seismologist
National Oceanography Centre, Southampton (NOCS)
University of Southampton
Waterfront Campus, European Way
Southampton SO14 3ZH
United Kingdom
bjc1g10@noc.soton.ac.uk

Patrick Fulton
Observatory/Physical Properties Specialist
Institute for Geophysics (UTIG)
University of Texas Austin
J.J. Pickle Research Campus, Building 196
10100 Burnet Road (R2200)
Austin TX 78758-4445
USA
pfulton@ig.utexas.edu

Takehiro Hirose
Physical Properties Specialist
Kochi Institute for Core Sample Research
Japan Agency for Marine-Earth Science and Technology
200 Monobe Otsu, Nankoku City
Kochi 783-8502
Japan
hiroset@jamstec.go.jp

Matt Ikari
Physical Properties Specialist
Center for Marine Environmental Science (MARUM)
University of Bremen
Leobener Strasse
D-28359 Bremen
Germany
mikari@marum.de

Tsuyoshi Ishikawa
Inorganic Geochemist
Kochi Institute for Core Sample Research
Japan Agency for Marine-Earth Science and Technology
200 Monobe Otsu, Nankoku City
Kochi 783-8502
Japan
t-ishik@jamstec.go.jp

Tamara Jeppson
Logging Scientist/Physical Properties Specialist
University of Wisconsin-Madison
Department of Geoscience
1215 West Dayton Street
Madison WI 53706
USA
tnjeppson@gmail.com

Jun Kameda
Sedimentologist
The University of Tokyo
Department of Earth and Planetary Science
7-3-1 Hongo, Bunkyo-ku
Tokyo 113-0033
Japan
kameda@eps.s.u-tokyo.ac.jp

James Kirkpatrick
Structural Geologist
Department of Earth and Marine Science
University of California, Santa Cruz
Santa Cruz CA 95064
USA
jkirkpat@ucsc.edu

Weiren Lin
Logging Scientist
Kochi Institute for Core Sample Research
Japan Agency for Marine-Earth Science and Technology
200 Monobe Otsu, Nankoku City
Kochi 783-8502
Japan
lin@jamstec.go.jp

Toshiaki Mishima
Paleomagnetist
Graduate School of Science
Osaka City University
3-3-138 Sugimoto Sumiyoshi-ku
Osaka City, Osaka 558-8585
Japan
mishima@sci.osaka-cu.ac.jp

J. Casey Moore
Sedimentologist/Logging Scientist
Research Professor Earth and Planetary Sciences
University of California, Santa Cruz
Santa Cruz CA 95064
USA
casey@ucsc.edu

Yasuyuki Nakamura
Seismologist/Physical Properties Specialist
Institute for Research on Earth Evolution (IFREE)
Japan Agency for Marine-Earth Science and Technology
3173-25 Showa-machi, Kanazawa-ku
Yokohama, Kanagawa 236-0001
Japan
yasu@jamstec.go.jp

Christine Regalla
Structural Geologist
Department of Geosciences
The Pennsylvania State University
University Park PA 16802
USA
cregalla@psu.edu

Francesca Remitti
Structural Geologist
Dipartimento di Scienze della Terra
Università di Modena e Reggio Emilia
largo S. Eufemia, 19
41100 Modena
Italy
francesca.remitti@unimore.it

Christie Rowe
Structural Geologist
Earth and Planetary Sciences Department
McGill University
Frank Dawson Adams Building 130B
3450 University Street
Montreal QC H3A 0E8
Canada
christie.rowe@mcgill.ca

James Sample
Inorganic Geochemist
Program in Geology
School of Earth Sciences and Environmental Sustainability
Northern Arizona University
Flagstaff AZ 86011-4099
USA
james.sample@nau.edu

Tianhaozhe Sun
Observatory/Physical Properties Specialist
University of Victoria
School of Earth and Ocean Sciences
Bob Wright Centre A405
PO Box 1700 STN CSC
Victoria BC V8W 2Y2
Canada
thzsun@uvic.ca

Ken Takai
Microbiologist
Subsurface Geobiology Advanced Research Project and Precambrian Ecosystem Laboratory
Extraterrestrial Life from Dark Universe
Japan Agency for Marine-Earth Science and Technology
2-15 Natsushima-cho, Yokosuka
Kanagawa 237-0061
Japan
kent@jamstec.go.jp

Virginia Toy
Structural Geologist
Department of Geology
University of Otago
360 Leith Walk
Dunedin 9054
New Zealand
virginia.toy@otago.ac.nz

Kohtaro Ujiie
Structural Geologist
Graduate School of Life and Environmental Sciences
University of Tsukuba
1-1-1 Tennodai
Tsukuba 305-0006
Japan
kujiie@geol.tsukuba.ac.jp

Monica Wolfson
Sedimentologist/Seismologist
Center for Coastal and Ocean Mapping Joint Hydrographic Center
University of New Hampshire
24 Colovos Road
Durham NH 03824
USA
mwolfson@ccom.unh.edu

Tao Yang
Paleomagnetist
Institute of Geophysics
China Earthquake Administration
No. 5 Minzu Daxue South Road
Haidian District
Beijing 100081
China
yangtao@cea-igp.ac.cn

Expedition 343T scientists

James J. Mori
Co-Chief Scientist
Earthquake Hazards Division
Disaster Prevention Research Institute
Kyoto University
Gokasho, Uji
Kyoto 611-0011
Japan
mori@eqh.dpri.kyoto-u.ac.jp

Patrick Fulton
Observatory/Physical Properties Specialist
Institute for Geophysics (UTIG)
University of Texas Austin
J.J. Pickle Research Campus, Building 196
10100 Burnet Road (R2200)
Austin TX 78758-4445
USA
pfulton@ig.utexas.edu

Nobuhisa Eguchi
Expedition Project Manager/Staff Scientist
Center for Deep Earth Exploration
Japan Agency for Marine-Earth Science and Technology
3173-25 Showa-machi, Kanazawa-ku
Yokohama, Kanagawa 236-0001
Japan
neguchi@jamstec.go.jp

Scientific observer (Expedition 343/343T)

Emily Brodsky
Seismology Laboratory
Earth and Marine Science C370
University of California, Santa Cruz
Santa Cruz CA 95064
USA
brodsky@pmc.ucsc.edu

Outreach specialist (Expedition 343)

Charna Meth
Associate Director
U.S. Science Support Program
The Consortium for Ocean Leadership
1201 New York Avenue, Northwest, Suite 400
Washington DC 20005
USA
cmeth@oceanleadership.org

Invited scientist (Expedition 343)

Kuo-Fong Ma
Professor
Department of Earth Sciences and Institute of Geophysics
National Central University
Zhong Da Road 300
Chung-Li, 32054
Taiwan
fong@eqkc.earth.ncu.edu.tw

Shipboard personnel and technical representatives

Captains (Mantle Quest Japan)
Yasushi Minoura
Yuji Onda

Offshore Installation Managers (Mantle Quest Japan)
Peter Hetherington
Masayuki Kawasaki

Operations Superintendents (CDEX)
Tomokazu Saruhashi
Ikuo Sawada

Drilling Engineers (CDEX)
Daiji Ikenomoto
Sho Kataoka
Yasuhiro Kawano
Tadashi Otani

Assistant Expedition Project Manager (CDEX)
Lena Maeda

Laboratory Officers (Marine Works Japan)
Satoshi Hirano
Tomoyuki Tanaka

Assistant Laboratory Officers (Marine Works Japan)
Toru Fujiki
Shunsuke Miyabe
Soichi Moriya

Curators (Marine Works Japan)
Yohei Arakawa
Masaru Yasunaga

Laboratory Technicians (Marine Works Japan)
Nobuhiro Anraku
Akihiko Fujihara
Yuji Fuwa
Kazuki Harumoto
Kentaro Hatakeda
Yuya Hitomi
Hiroshi Hoshino
Tatsuya Kawai
Sayaka Kawamura
Yoshiki Kido
Shunsuke Miyabe
Yuki Miyajuma
Takumi Mori
Hiroaki Muraki
Yukihiko Nakano
Masahiro Nishimura
Atsushi Ohashi
Satomi Saito
Masumi Sakaguchi
Kiyoshi Shiono
Hiromichi Soejima
Tatsuya Sugiyama
Takahiro Suzuki
Yasumi Yamada
Nagisa Yamamoto
Kanako Yoshida

Observatory Engineers (CDEX)
Masanori Kyo
Yasuhiro Nanba
Yuichi Shinmoto

Operation Geologists (CDEX)
Kan Aoike
Takamitsu Sugihara

Publications Assistant (Marine Works Japan)
Yoko Isoda

Tool Pusher/Coring Supervisor (Mantle Quest Japan)
Kevin Beamish
Geoff Cook
Teruyuki Koyama
Paul Thornton

Abstract

The main science goal of the Japan Trench Fast Drilling Project (JFAST) is to understand the physical mechanisms and dynamics of large slip earthquakes, which is fundamental to understanding the huge tsunami that caused extensive damage during the 2011 Tohoku earthquake. Specifically, the level of frictional stress during the earthquake rupture and the physical characteristics of the fault zone are investigated through drilling. The objectives of JFAST include locating the fault that ruptured during the Tohoku event using logging while drilling (LWD); characterizing the composition, architecture, and fundamental mechanisms of dynamic frictional slip and healing processes along the fault by taking core samples; and estimating the frictional heat and stress within and around the fault zone by placing a temperature measurement observatory across the fault.

During the main JFAST expedition (Integrated Ocean Drilling Program [IODP] Expedition 343 in April and May 2012), LWD was completed in a borehole drilled to 850.5 meters below seafloor (mbsf) (total depth [TD] = 7740 meters below sea level [mbsl]), and a coring hole was drilled to 844.5 mbsf (TD = 7734 mbsl) to acquire 21 cores that spanned the two main fault targets. Because of delays associated with severe weather and technical challenges of operating in great water depths, installation of the observatories for temperature and pressure measurements was not completed during the main expedition; however, temperature sensors were successfully deployed during a short technical extension of JFAST, IODP Expedition 343T (JFAST II), in July 2012.

Principal results of Expedition 343/343T include the following:

1. The overall structure at the drill site consists of a prism of faulted and folded clayey to silty mudstones above, and in fault contact (at ~820 mbsf) with, a largely undeformed, relatively thin sequence of hemipelagic and pelagic sediments that were deposited on top of the incoming Pacific plate. The primary constituents of the mudstones that make up the prism are terrigenous silt and clay, vitric ash, and biogenic silica. The fault contact, interpreted as the plate boundary décollement, is defined by a subhorizontal, <5 m thick zone of highly sheared clay that displays penetrative scaly fabric and localized slip surfaces.
2. Faults and bedding are variable in dip magnitude, but faults and bedding at all depths in the prism show a preferred northeast strike direction reflecting horizontal contraction and local extension (at shallower depths) approximately parallel to the plate convergence direction.

3. Borehole breakouts are evident in image logs from the LWD hole and indicate several different in situ stress domains along the borehole. At shallow depths (from <200 to ~500 mbsf), the maximum horizontal compressive stress (S_{Hmax}) is variable and shows a complicated pattern. At deeper levels in the prism (537–820 mbsf), S_{Hmax} displays a single preferred orientation approximately 20° clockwise from the convergence direction.
4. Fault slip during the 2011 event and other past earthquakes likely occurred on the plate boundary décollement. However, slip on other faults cutting the prism could have also occurred during the Tohoku event. One possible location of recent fault slip is identified at ~700 mbsf on the basis of a local H_2, methane, and chlorinity anomaly. Several core samples from a fractured and brecciated zone at ~720 mbsf contain faults, the largest of which is a high-angle reverse fault that occurs at the same depth as a low-resistivity feature identified in image logs. The fault at ~720 mbsf and the décollement at ~820 mbsf are the two primary targets for the temperature measurement observatory.
5. Successful recovery of ~1 m of highly sheared clay and neighboring sediments from the plate boundary décollement provide plenty of material for mechanical and physical properties testing, as well as for geochemical, mineralogical, and microstructural analyses. Three special interest structural whole-round samples taken from the sheared clay of the décollement, as well as two other structural whole rounds capturing secondary faults, will provide material for coordinated nondestructive and destructive investigations of structure, chemistry, and mineralogy of the faulted sediments.
6. An observatory consisting of 55 temperature sensors and autonomous data loggers was successfully installed across the two fault targets. These instruments are monitoring the temperature distribution across the lower portion of the borehole to estimate the amount of frictional heat dissipated along the slip zone of the Tohoku earthquake in order to estimate the level of dynamic frictional strength during the earthquake.

Introduction

The 2011 Tohoku earthquake (Mw 9.0) and accompanying tsunami devastated much of the northeast coast of Honshu, Japan, and highlighted many of the poorly understood aspects of how great earthquakes occur. An important aspect of the event was the very large amount of slip (~50 m) on the shallow portion of the megathrust,

which is the largest displacement ever recorded in an earthquake (Fujiwara et al., 2011; Ito et al., 2011; Sato et al., 2011). Based on current ideas of the rheology and behavior of shallow faults, the large amount of displacement and its location, which reached the trench, was not anticipated (Ammon et al., 2011; Avouac, 2011; Ide et al., 2011). The huge amount of movement on the shallow portion of the megathrust and associated displacement of the ocean floor was the main cause of the destructive tsunami (Ito et al., 2011; Ide et al., 2011; Fujii et al., 2011).

The scientific community needs to learn as much as possible from this extreme event. Specifically, we want to clarify the physical conditions and state of stress that enabled the large slip to occur. We also hope to identify the effects of the earthquake on the fault zone so that we can identify the recent event and other events in the geological record. With understanding of the physical conditions on the fault zone and knowledge of past earthquakes, we will be able to improve evaluations of future occurrences of large tsunamis in the Tohoku region, as well as for other subduction zones around the world (e.g., Ozawa et al., 2011; Ammon et al., 2011).

An important aspect of Integrated Ocean Drilling Program (IODP) Expedition 343 (Japan Trench Fast Drilling Project [JFAST]) is the priority on collecting time-dependent observations of fault properties following a large earthquake. Measurements of the decaying temperature of the fault zone, as well as analyses of the changing stress and chemical properties of the fault rocks, are important observations that need to be made soon after the earthquake (Brodsky et al., 2009; Fulton et al., 2010). The scheduling of this expedition within 13 months following the earthquake reflects the rapid response taken by IODP to provide scientific information about large-scale geohazards that severely impact our societies.

Background

Geological setting

The 2011 Tohoku earthquake occurred on the megathrust fault surface west of the Japan Trench where the Pacific plate of Cretaceous age subducts below Honshu Island. The subduction zone is characterized by a relatively rapid convergence rate of ~85 mm/y (e.g., Apel et al., 2006; DeMets et al., 2010; Argus et al., 2011), a high rate of seismic activity, and a deep trench (Kanamori et al., 2006; Hashimoto et al., 2009; Simons et al., 2011). The historical record for the region includes 13 Mw 7 and 5 Mw 8 earthquakes over the last 400 years. The convergent margin of the Japan Trench dis-

plays the features generally associated with subduction erosion (von Huene et al., 1994, 2004; Tsuru et al., 2000), specifically, evidence of subsidence in the Neogene with associated extensional faulting in the middle slope region, horst and graben structures in the upper portion of the subducting plate, and a relatively small frontal prism (5–15 km wide) containing landward-dipping reflectors and a backstop bounding the frontal prism on the landward side.

The structure and lithology of the forearc region of northern Japan were investigated during Deep Sea Drilling Project (DSDP) Legs 56 and 57 (Arthur and Adelseck, 1980), and later observatories were established in the forearc during Ocean Drilling Program (ODP) Leg 186 (Sacks, Suyehiro, Acton, et al., 2000). ODP Leg 186 Sites 1150 and 1151 are located above the region of large fault slip during the Tohoku earthquake, ~100 km north of the epicenter (e.g., Lin et al., 2011). DSDP Leg 56 and 57 Sites 434–441 are located approximately 50–100 km further north (Fig. **F1**). In this region, the Japan Trench system consists of a deep-sea terrace, inner trench slope, midslope terrace, trench lower slope, the trench, and outer trench slope (Arthur and Adelseck 1980; Tsuru et al., 2002). A forearc basin formed at the deep-sea terrace contains sequences of Neogene sediments as thick as 5 km overlying a Cretaceous unconformity, which correlates with a regional unconformity and relates to geologic features on land. The overlying sediments extend trenchward through the midslope terrace to the backstop boundary, and the frontal prism forms the trench lower slope (e.g., Tsuru et al., 2000). Seismic profiling indicates the structure in the northern Japan Trench is similar through the region to the south that ruptured during the Tohoku event (Tsuru et al., 2002).

The frontal prism is characterized by lower seismic velocity than the region landward of the backstop, and the prism displays disrupted-to-chaotic reflection patterns that likely indicate strong deformation (e.g., Tsuru et al., 2000). Coring of the toe region of the frontal prism at Site 434 revealed the prism is composed of a highly disrupted, very uniform hemipelagic deposit (Shipboard Scientific Party, 1980a). The major constituents are terrigenous silty clay, biogenic silica, and vitric ash. Biostratigraphic observations indicate structural complexity in the prism with repetition of assemblages that could record slumping, sliding, and faulting. Significant induration of the sediments occurs at depths below ~100 m, and the mudstones recovered are highly fractured with slickensided faces. The highly fractured and disrupted structure contributed to the difficulties of coring and poor core recovery at Site 434.

Seismic studies/Site survey

The offshore Tohoku region is well characterized from decades of data collection, including some high-resolution surveys of bathymetric and seismic reflection data taken after the 2011 Tohoku earthquake (Kodaira et al., 2012; Fujiwara et al., 2011). A differential bathymetry analysis across the trench axis eastward of the hypocentral area, using data collected along the same track before and after the earthquake, shows large topographical changes on the landward side of the trench. From analysis of differential bathymetry, Fujiwara et al. (2011) demonstrate approximately 50 m of horizontal movement toward the southeast and 10 m of upward movement during the earthquake. In addition, a large submarine landslide scarp on the lower trench wall and associated slump deposits in the trench are indicated by the distinct negative and positive seafloor elevation changes at the trench. A critical result is that the coseismic displacement of the 2011 Tohoku earthquake extended all the way to the landslide scarp, if not to the trench axis proper (Kodaira et al., 2012). The pervasive and similar magnitude of displacement along the profile shows that the frontal prism was displaced as a coherent unit along a fairly uniform dipping detachment surface. Analysis of other data sets also points to coseismic slip on the order of 50 m that extends to the trench (e.g., Ito et al., 2011; Ide et al., 2011; Simons et al., 2011; Fujii et al., 2011).

Based on the above observations and the geometric continuity with the deeper main detachment surface, the plate interface is considered to be the most likely fault surface of large displacement during the earthquake (e.g., Ito et al., 2011; Kodaira et al., 2012).

Japan Agency for Marine-Earth Science and Technology (JAMSTEC) carried out high-resolution seismic surveys in the area of the large seafloor displacement. Multichannel seismic data perpendicular to the trench axis along Line HD33B (Fig. **F2**) show a strong reflector at ~800 meters below seafloor (mbsf) that is thought to be the sediment/basalt interface of the subducting Pacific plate. A weak reflector about 50 m above this strong reflector is interpreted as the megathrust fault zone and is the main target of JFAST drilling.

The selection of the drilling site was constrained by a maximum penetration depth of 1000 mbsf for riserless drilling and a maximum water depth of 7000 m. In general, the plate interface shallows toward the trench but the water deepens. Generally, the plate interface at a water depth of ~7000 m is shallower near 38°N and deeper further north. On the basis of existing seismic data, the primary site (JFAST-3) was identified

as a location that minimizes both water depth and fault depth below the seafloor (Fig. **F3**).

Scientific objectives and operational strategy

The main goal of Expedition 343 is to understand the stress conditions and physical characteristics of the fault that allow very large fault slip to occur near the trench. The following specific science objectives reflect the unique possibilities provided by rapid response drilling into a fault following a large earthquake. The shallow distribution of large slip for the Tohoku earthquake provides an unprecedented opportunity to directly access a fault that has recently moved tens of meters. As outlined in the report from the International Continental Scientific Drilling Program/Southern California Earthquake Center international workshop on rapid response drilling (Brodsky et al., 2009), fundamental questions regarding stress, faulting-related fluid flow, and the structural and mechanical characteristics of the earthquake rupture zone can be addressed uniquely through rapid response drilling.

The science questions and strategies for addressing them are as follows:

1. What was the stress state on the fault that controls rupture during the earthquake, and was the shear stress on the fault completely released?
   - Dynamic friction during the rupture: potentially the most significant result of this project will be determining a value for the dynamic frictional stress. Measurements of the time-decaying temperature will be used to estimate the frictional heat produced at the time of the earthquake, which can be used to infer the level of dynamic frictional stress.
   - Rupture to the toe of the sedimentary wedge: past thinking was that sediments in this region are weak and rate strengthening, so earthquake instability should not nucleate or easily propagate through this region. Measurements of current stress and stress during the earthquake can be used to explore different models to explain how dynamic slip occurred. Hydrogeological measurements can also help constrain the healing process of the fault.
2. What are the characteristics of large earthquakes in the fault zone, and how can we distinguish recent and geologic-past events in fault zone?
   - Core analyses: detailed studies of textures and small-scale structures of core samples from the fault zone will be used to infer the role of fluids and pressurization during rupture. We will look for evidence of melting or other processes that contribute to dynamic strength reduction. Trace element chemistry and

other physical and geochemical anomalies will be used to estimate the thermal history of the recent and past events.

- Laboratory experiments: high-speed friction and petrophysical experiments on fault material can be used to characterize the frictional behavior of the fault.

Secondary science objectives include carrying out other geological, geochemical, and microbiological observations to the greatest extent possible during drilling in accordance with the IODP Measurements guidelines (**www.iodp.org/program-policies/**). As a specific example, there is some evidence that great amounts of hydrogen may be released at the time of large faulting (e.g., Kita et al., 1982). The production of hydrogen may stimulate microbiological activity; thus, samples of the fault may contain records of biogeochemical and microbiological processes.

The primary science objectives are closely aligned with the Initiative: Seismogenic Zone of the IODP *Initial Science Plan*. This initiative advocates subduction zone studies that include investigating the behavior of rocks and sediments to better understand the fault zone and integration with studies of earthquake mechanics. Furthermore, this project directly addresses Challenge 12 of the IODP *Science Plan for 2013–2023*: "What mechanisms control the occurrence of destructive earthquakes, landslides, and tsunami?"

Strategy/Drilling plan

Details regarding the original drilling plan are available in Mori et al. (2012), but the general planned sequence of drilling was as follows:

1. Drilling the pilot hole with logging while drilling (LWD)/measurement while drilling (MWD) to total depth (TD), planned for ~900 mbsf;
2. Running casing and a completion assembly (including long-term temperature monitoring with the autonomous string) in the LWD/MWD hole to ~900 mbsf (casing to 50 m below fault, ~900 m);
3. Drilling a second hole with rotary coring barrel (RCB) drilling (with center bit) to ~500 mbsf and continuation with RCB coring to ~900 mbsf; and
4. Running casing and a completion assembly for the second hole (including long-term temperature and pressure monitoring with the telemetered string) to ~900 mbsf (casing to 50 m below fault, ~900 m).

Principal results/Site summaries

Although severe weather and failure of various equipment delayed operations at Site C0019, nothing occurred that would require abandonment of the primary goals of the expedition and shifting to contingency sites. Accordingly, all drilling and coring activities occurred at IODP Site C0019 (Fig. **F3**) for the duration of the expedition. During JFAST (Expedition 343) in April and May 2012, the LWD/MWD pilot was drilled in Hole C0019B to a TD of 850.5 mbsf (Fig. **F4**). In preparation for deploying the autonomous temperature measurement observatory, a wellhead and 20 inch casing were successfully set in Hole C0019D. Finally, the coring hole was successfully completed in Hole C0019E where spot cores were acquired from various depths to the TD of 844.5 mbsf. The LWD/MWD and coring holes were blind-spudded with an estimated 5 m of separation at the seafloor. During JFAST II (IODP Expedition 343T) in July 2012, the wellhead in Hole C0019D was successfully reentered to extend the borehole to a TD of 854.8 mbsf (Fig. **F4**). Subsequently, the 4½ inch casing containing the miniature temperature logger (MTL) autonomous observatory was installed and the observatory was completed (Table **T1**).

Site C0019

Geophysical logging

Hole C0019B was drilled to 850.5 mbsf, and the entire hole was successfully logged using a LWD/MWD assembly. The logging tools used during Expedition 343 include two of Schlumberger's VISION series tools, namely geoVISION and arcVISION, in addition to their MWD TeleScope tool. Four logging units were defined on the variability of log responses (Fig. **F5**). In the upper 800 m of the borehole, in logging Units I and II, the overall responses of both gamma ray and resistivity increase with depth. In the gamma ray log this trend is broken by significant low values that occur at 168 and 535 mbsf. There is evidence of potential cyclicity in the resistivity log response, and the resistivity-at-the-bit (RAB) images also show multiple zones transitioning from darker, more conductive layers to lighter, more resistive bands with depth. Similarly, the abundance of borehole breakouts is variable with low occurrences below 230, 470, and 730 mbsf. The patterns described above could infer sediment packages of different lithologies or an overall homogeneous sediment unit cut by thrust faults (producing repeated sediment packages), or a combination of these. The gamma ray and resistivity log responses from the upper 800 m of Hole C0019B compare favorably to those of diatomaceous muds that were recovered and logged at neighboring ODP

Sites 1150 and 1151 ~100 km away (Sacks, Suyehiro, Acton, et al., 2000) and at DSDP Sites 436 and 434 (Shipboard Scientific Party, 1980a, 1980b).

Logging Unit III (820.6–835.9 mbsf) is defined by a significant increase in gamma ray intensity relative to the units above that remains high for 16 m before dropping sharply (Fig. **F5**). RAB images also indicate this unit is more conductive compared to the units above and below. Such log response could indicate a clay-rich unit, possibly similar to the brown clay unit recovered from Leg 56 Site 436 (Shipboard Scientific Party, 1980b). Logging Unit IV (835.9–850 mbsf) is characterized overall by low gamma ray and high resistivity values. RAB images primarily show regions of very high resistivity in layers and patches throughout this logging unit. The resistivity and gamma response is consistent with lithologies such as chert, and RAB images may indicate some interbedding of chert and a more conductive material. Chert was also observed below the brown clay at Site 436 (Shipboard Scientific Party, 1980b).

Bedding and fracture occurrence and orientation were determined from borehole resistivity images (Fig. **F6**). Three structural domains may be defined on the basis of bedding dip distributions: (1) upper frontal prism (0–275 mbsf) with more gently inclined bedding, (2) lower frontal prism (276–820 mbsf) with variable and steeply dipping beds, and (3) base section (820 mbsf to base of hole) with shallow to horizontal bedding. The poles-to-bedding in the lower frontal prism are consistent with cylindrical folding with a mean axial trend of 030°, which is about 20° northeast of a line parallel to the regional slope and nearly normal to the convergence direction of 292° (DeMets et al., 2010; Argus et al., 2011). Structural Domain 1 shows sparse fractures, whereas fractures are more numerous in Domains 2 and 3. Similar to bedding, the strike of fractures displays a preferred northwest orientation. A zone of enhanced fracturing occurs around a significant conductive feature at 720 mbsf. The feature is shown as a large negative excursion in the standard logs and a dark band in the RAB images, which may reflect a zone of faulting (Fig. **F5**). This feature was regarded as a potential site of the Tohoku earthquake rupture and was targeted for coring; the feature is hereafter referred to as the 720 fault.

Another probable fault was identified at 820 mbsf between structural Domains 2 and 3 and between logging Units II and III, hereafter referred to as the 820 fault. The structural transition resembles that of a classic décollement, with variably dipping beds above and shallow dipping beds below that are sitting above the basaltic crust (Fig. **F6**), and interpreted as a brown clay layer and chert characteristic of the incoming oceanic plate of the north Pacific Ocean (Shipboard Scientific Party, 1980b).

Breakouts were identified in the image logs of Hole C0019B and are found to occur over a broad depth range in logging Units I and II and structural Domains 1 and 2 (Fig. F7). Breakout distributions display preferred orientations that vary with depth. The mean azimuth of breakouts in the deeper portion of the hole (537–820 mbsf) is 049° and the standard deviation is 23°. Thus the maximum horizontal compressive stress orientation can be interpreted as 319° ± 23° at the base of the prism. At immediate depths, the breakouts are less frequent and orientations are highly variable. In the shallower portion of the borehole, the orientation of breakout azimuth progressively rotates clockwise down to 140 mbsf and then rotates back counterclockwise, suggesting the presence of a discontinuity, perhaps a fault. This is supported by a conductive peak in the resistivity logs. Changes in bedding dips are also consistent with the presence of a discontinuity at this depth.

Downhole measurements and observatory

No observatory components were deployed during the main portion of Expedition 343; however, some downhole observations were made to measure temperature and pressure using 1–3 of the MTLs (TDR2050) placed in the inner core barrel of the RCB coring assembly. Deplugger operations typically use the inner core barrel with a special center adaptor to clear the RCB bit; we used the inner barrel to hold the MTL sensors for in situ pressure and temperature measurements. The inner core barrel containing the instruments was deployed by a free-fall release down the drill pipe in a procedure that was developed onboard during the expedition. Three different measurement runs were completed on 12 May, 16 May, and 22–24 May.

Temperature measurements made within the borehole were highly affected by drilling operations, particularly measurements recorded during pumping and circulation. Although pumping and circulation was stopped prior to making the third run, we did not expect the borehole temperature to have equilibrated by the time measurements were taken, and this was confirmed by observations that the temperature changed with time even though the pipe was fixed in position.

Pressure measurements showed significant fluctuations, reflecting changes in depth of the instrument with time. The dominant signal indicated cyclic changes in depth consistent with ship heave. However, additional pressure variations were recorded that implied depth variations of much greater magnitude than the heave. It was determined that these large variations in pressure (depth) reflected vertical oscillations that were triggered by rapid accelerations of the drill stem or core line at the ship, as occurs for example during addition or removal of pipe stands and retrieval of the in-

ner barrel holding the MTL sensors. This effect is magnified during free hanging of the extremely long drill stem and core line that were employed for the deepwater operations of this expedition.

During Expedition 343T in July, the autonomous temperature observatory consisting of MTLs was successfully deployed in Hole C0019B (Fig. F8). The instrument string of 55 MTLs was suspended in 4½ inch pipe from a hanger at the wellhead. Three types of MTLs from two different manufacturers were used, which differed in data storage volume. Also, some of the instruments included pressure sensors for accurate estimates of water depth. The sensors are designed to monitor the changing temperature at sample intervals of 10 s to 10 min over several months until their retrieval, which is scheduled for October 2012 or February 2013. Also, two of the instruments were programmed to turn on at high sample rates during the time of the anticipated retrieval, in order to obtain a temperature profile during pullout. The MTLs are distributed over about 550 m with dense spacing of 1.5 m near the 820 fault. Because of the possibility of postseismic slip on the fault that may deform the borehole and cut the instrument string, weak links that can break at designated positions were interspersed along the instrument string to help minimize loss of MTLs.

Lithology

As a result of time constraints, a total of 21 coring runs at four depths were completed. Lithologic Unit 1 was sampled by a single spot core taken from the 176.5–186.0 mbsf interval (Fig. F9). The core consists of a medium olive-gray siliceous mudstone with secondary lithologies including isolated, few millimeter to 2 cm thick layers of yellowish gray ash and dark gray to black, millimeter-scale laminations with gradational contacts. The siliceous mudstone is dominated by abundant clay- to silt-sized siliciclastic material and includes abundant siliceous microfossils (diatoms, sponge spicules, and radiolarians) and common ash shards.

Lithologic Unit 2 was sampled by two coring runs taken from the interval 648.0–660.5 mbsf. Recovered sediment comprises bluish gray ashy mudstone and grayish brown ashy mudstone, both of which are heavily brecciated and thoroughly mixed throughout by drilling and recovery processes. Both mudstones contain dominant siliciclastic grains, common volcaniclastic grains, and biogenic fragments that are present and occasionally common.

The sediments of lithologic Unit 3 were relatively well sampled from 13 coring runs covering intervals 688.5–729.0 and 770–821.5 mbsf (Fig. F9). Unit 3 comprises four

dominant lithologies, an olive-brown-gray ashy mudstone, a dark gray mudstone with black interlayers, a clay-rich mudstone, and a dark gray mudstone with abundant pyrite. These units are interbedded on a meter scale with occasional centimeter-scale interlayers and intermittent centimeter-scale clay and silt beds. All lithologies are dominated by siliciclastic material and contain trace or present siliceous microfossils and fossil fragments, with rare horizons containing up to 15% siliceous fragments. Ash is abundant in the ashy mudstone, but otherwise ash layers are rare and ash content decreases significantly downsection below the ashy mudstone. X-ray diffraction data show the overall quartz, feldspar, and clay content of Unit 3 is generally consistent throughout the section except for discrete clay and silt beds. Unit 3 has a much higher component of siliciclastic material and a lesser component of volcanic and siliceous grains than Unit 1. Unit 3 contains none of the grayish brown or bluish gray ashy mudstones of Unit 2. Unit 3 reflects a more terrigenous environment of accumulation than Units 1 and 2 and a time of lesser accumulation of siliceous microfossils and increased distance from, or lesser activity of, volcanic sources.

Unit 4 occurs in only one core taken from the interval 821.5–824.0 mbsf. Unit 4 consists of strongly deformed clays that are pervasively sheared, forming sharp strongly aligned phacoids with polished, striated surfaces defining a scaly fabric. Two main components can be recognized from visual inspection and smear slide analysis: a red-brown clay and a dark brown to black clay. The reddish brown clay is composed predominantly of clay minerals with rare coarser grains and vitric grains, whereas the dark clay is composed mainly of dark red-brown clay minerals probably mixed with Fe or Mn oxides/hydroxides. Sections 0.5–4 cm thick of reddish to dark brown and black clay alternate at the top of the core. A 13 cm section of gray mudstone is enclosed inside the clay. Downsection from the mudstone interval, dark brown to black clay is dominant. The foliation defined by the scaly fabric varies from horizontal to ~25° inclination. The upper and lower contacts of Unit 4 with Unit 3 above and Unit 5 below were not captured in the recovered core section.

Unit 5 is a yellowish to grayish brown mudstone composed of dominant siliciclastic grains, minor volcaniclastic grains, and trace siliceous microfossils (radiolarians). The siliciclastic component of the rock is predominantly clayey in the upper part of the unit (>60% clay and <40% silt) and becomes more silty in the lower part (<60% clay, >40% silt) with trace sand. Bedding is often indistinct but is loosely defined by alignment of the long axes of the elliptical lenses of all colors. The contact between Units 5 and 6 is contained in Core 343-C0019E-20R, and it appears conformable and is likely stratigraphic. The overall nature of the unit, particularly the dominance of silt

in the lower portion, indicates a significant influx of siliciclastic and terrigenous material relative to the biogenic and pelagic clay deposits in Unit 6 below.

Unit 6 comprises laminar yellow-brown and dark brown clay with occasional pink, red-brown, and white laminae. It is 0.65 m thick, occurs within the lower portion of Core 343-C0019E-20R, and is in contact with Unit 5 above and Unit 7 below. The unit consists of >80% siliclastic grains, with <10% volcanic grains and trace–10% siliceous microfossils. Diatoms are not observed in this interval, but radiolarians are present. More than 75% of the material falls in the clay grain size fraction. The bottom section consists of green to light green clays and gradationally transforms into chert (Unit 7). Radiolarian molds are present in the basal section of Unit 6. Unit 6 is interpreted as pelagic clay deposited on the incoming Pacific plate.

Unit 7 consists of yellow-brown and chocolate-brown laminar chert that occurs as fragments at the base of Core 343-C0019E-20R and in Core 21R, taken from the interval 831–844.5 mbsf (TD). Similarity in color and lamination of the chert to that observed in the overlying clay, and the intermixing of clay and chert observed in Cores 20R and 21R, suggest that the underlying chert is formed by silicification of the clay. The transition from the pelagic clays in Unit 6 to the chert in Unit 7 was not sampled directly, but the presence of chert nodules and intercalated chert layers within Unit 6 suggests the transition is a diagenetic front. Unit 7 is correlated to the chert recovered in the incoming Pacific plate during Leg 56 at Site 436 (Shipboard Scientific Party, 1980b). Similar to Leg 56, the fine-scale laminations within in the chert represent the only primary sedimentary structures, implying minimal transport and reworking of the clays prior to silicification.

Site 436 is located off Northern Honshu and represents the most proximal drilling site that can be used as a reference for the section cored at Site C00019. Site 436 consists of three lithologic units: Unit 1, vitric diatomaceous silty clay and claystone; Unit 2, radiolarian diatomaceous claystone; and Unit 3, pelagic clay with chert and porcellanite. Site 436 Units 1 and 2 are lithologically similar to Site C0019 Units 1–3, which are composed of mudstone, siliceous mudstone, and locally ashy mudstone. This lithologic description is very general and does not necessarily imply a direct correlation between the units in Hole C0019E and the incoming plate strata. Site C0019 Units 4–7 correlate to Site 436 Unit 3. There are direct matches between the brown clay, the multicolored clays, and the chert between these unit correlations. For example, chert in Units 6 and 7 closely resembles descriptions of chert at Site 436 interval 378.5–397.5 mbsf, in which scarce Albian–Cenomanian radiolarians indicate a Cretaceous

depositional age (Shipboard Scientific Party, 1980b). However, an equivalent of Site C0019 Unit 5 (brown mudstone) was not identified in Site 436 Unit 3. The lithology of Site C0019 Unit 5 could represent a stratigraphic variation between the two holes or could be structurally emplaced from the upper plate at Site C0019. The former interpretation is favored because of the absence of a sheared basal contact of Unit 5 at Site C0019.

Structural geology

Investigation of structures in core samples through combined X-ray computed tomography (CT) imaging and visual observation provided a wealth of data that both verify and extend the structural data derived from the LWD/MWD borehole logs. Within the intervals sampled by coring, numerous orientation measurements of bedding and fractures and orientation and kinematics of faults were obtained. Unfortunately, appropriate paleomagnetic poles to correct bedding strike to true azimuths have not yet been determined, so here we concentrate on dip magnitudes and shear sense indicators.

In core samples from lithologic Unit 1 in structural Domain 1, direct measurement of bedding indicates a magnitude of dip of 30°. Faults are diffuse, narrow (few millimeters thick) zones of deformed sediment with similar composition to the adjacent sediment. In the X-ray CT images, faults are tabular zones of material with high CT number (which appear as bight features), several millimeters thick, that truncate and offset worm burrows and bedding they intersect. Fault surfaces in the core are polished and display slickenlines defined by aligned clay particles, which are correlated to bright planes. Of 10 mapped faults, all are dip-slip. Three are normal faults, and the shear sense of the others was not determined. Fault dip averages 66° ± 9°, ranging from 55° to 81°. Measured offsets are of the order of 1 cm, but several faults had offsets greater than the diameter of the core. Both bedding and fault dip determined from the core are consistent with bedding and fracture orientations determined from image logs.

Because of the extreme brecciation of core containing lithologic Unit 2, few structural measurements were possible. A single probable bedding surface that dips ~3° is marked by a dark band that grades gradually darker toward the top of the core. Additionally, five dip-slip faults were identified. Some were recognized in CT images as bright surfaces cutting burrows and were then located in core. Of the faults, one was inferred as a normal shear sense. Fault dip is variable, ranging from ~10° to steeper than 70°.

Coring from 688.5 to 729.0 and 770 to 821.5 mbsf sampled lithologic Unit 3 and structural Domain 2 across the 720 fault to the 820 fault. Core observations confirm the variation in bedding dip magnitude determined from the image logs but define some patterns in dip magnitude in particular intervals. Between 660 and 680 mbsf, bedding dips average 37° ± 20° and are variable through the entire interval. From ~770 to 790 mbsf, steeper dips dominate, including some potentially overturned intervals with very steep dips (average 64° ± 15°). From ~800 mbsf to the base of the unit at ~820 mbsf, moderate dips dominate (average 38° ± 11°).

The most common structures observed in Unit 3 over the depth intervals 688.5 to 729.0 and 770 to 821.5 mbsf are dark seams and dark bands. Dark seams are planar to curviplanar and are <1 mm in thickness (usually hairline ~100 µm width), whereas dark bands are tabular or curviplanar to irregular with their thickness ranging from <1 mm to 2–3 mm along their length. On the CT images, most dark seams and some dark bands are marked by bright seams and bright bands, respectively, with higher CT numbers than those of the surrounding material. The different characteristics of these features were investigated both visually and in X-ray CT imaging. The truncation and offset relationships and X-ray CT brightness properties suggest dark seams are likely solution surfaces or very thin shear surfaces, whereas dark bands are usually shear surfaces but may also rarely be bedding or bedding-parallel shear surfaces. The dip angles of these features are highly variable throughout and occur over a range of dips at each depth interval. However, overall low-angle faults are more prevalent deep in the section between 800 and 820 mbsf.

A noteworthy zone of fractured and brecciated sediment occurs between 719 and 725 mbsf. Over a 0.27 m interval centered around 719.85 mbsf, beds are crosscut and offset by a 15 mm thick, anastomosing, 60° dipping fault zone. This feature correlates quite closely with interval of low resistivity identified in resistivity image logs from the neighboring Hole C0019B (i.e., the 720 fault). From 719 to 725 mbsf (below the fault), the mudstone is broken into angular fragments ranging from 1 to 10 cm diameter along sets of inclined fractures that may be parallel to, or exploit, dark seams. The fractures are commonly polished and slickenlined and sharply cut burrows and the mottled texture and compositional layering in the mudstone. Stepped slickensides and drag of bedding along the fault indicates reverse shear sense.

Another notable fault (at 697.2 mbsf) was identified in CT images as a ~2–7 mm thick bright band that dips 10° with respect to a horizontal plane. The section above the bright band shows inclined fissility in homogeneous sediment, whereas fissility is ab-

sent in the section below, which is distinctively mottled, suggesting a slip magnitude sufficient to juxtapose different sedimentary layers. The interval including the bright band was taken as a structural whole-round sample because this interval is close to the location of an H_2 anomaly at 697.9 mbsf; the sample was not further described during the shipboard operations but will be the focus of some shore-based studies.

Unit 4 is only observed within, and makes up all of, Core 343-C0019E-17R. Structures in Unit 4 were identified from observation of the whole round and X-ray CT images. Most of the core is composed of clay with a variably intense scaly fabric. There is also an interval (0.22–0.34 m from the top of the section) of relatively intact and only slightly sheared mudstone with upper and lower boundaries in contact with the sheared clay. The intense scaly fabric within the clay is characterized by polished lustrous surfaces, commonly striated, enclosing narrow, variably shaped and sized lenses of less fissile material, termed phacoids. The major and intermediate axes of the phacoids define the dominant, pervasive foliation. In any observation section, the phacoids appear bounded by surfaces with two predominant orientations, but locally one surface orientation predominates. In the uppermost 22 cm of the core, phacoids are sometimes asymmetric when viewed in a section perpendicular to the foliation and parallel to the dip direction of the foliation; the observed asymmetry indicates reverse shear sense.

In general, phacoid size increases with depth in Unit 4; however, there are several abrupt, discontinuous changes in color and phacoid size implying compositional and structural layering parallel to the foliation. The most finely foliated scaly fabric is observed between 0 and 0.20 m, where the red-brown clay forms platy phacoids with minor axes <1 mm in length. Within this interval, a visibly obvious curviplanar contact juxtaposes the predominantly red-brown clay and predominantly dark brown to black clay. The contact surface is slightly wavy at the centimeter scale with amplitudes <1 mm; the foliation on either side is truncated without deflection at the contact. These features are consistent with a meters thick shear zone hosting mesoscopic-scale surfaces of localized slip.

The interval of intact mudstone bounded by the sheared clay layers above and below displays three major sets of intersecting dark seams, some of which offset each other by a few millimeters. The major dark seams are shallow dipping subparallel to the bounding surfaces. The deformation features on the mudstone interval are similar to those observed within lithologic Unit 3 in Core 343-C0019E-15R, as well as to the fracture sets that were opened during drilling in the top of Unit 5 (Cores 18R and

19R). Deformation of the mudstone may have occurred during shearing of the entire unit. Alternatively, because similar structures are observed in Units 3 and 5, the observed deformation could predate the incorporation of the mudstone as a tectonic lens within the sheared clay.

Overall, the sheared zone of clay displaying scaly fabrics in Core 343-C0019E-17R markedly contrasts with relatively coherent and much less deformed sediments recovered from above and below Core 17R. The fact that the primary bedding has been completely destroyed by shear deformation and a penetrative scaly fabric containing localized slip surfaces developed in the layer indicates it has accommodated significant shear displacement and constitutes the core of a major fault. The total thickness of the sheared clay layer is unknown because the upper and lower contacts were not recovered and recovery of Core 17R was 38.8%. If unrecovered intervals in Cores 16R–18R are also composed of sheared clay, the maximum thickness of the sheared zone is 4.86 m. Regardless of true thickness, the structure of the layer is compatible with displacement on the order of hundreds to thousands of meters of slip. Also compatible with significant displacement is the abrupt change in lithology and bedding dip across the interval of scaly clay; the sediments in the hanging wall show moderate dip magnitudes and those in the footwall are subhorizontal. Moreover, the footwall strata are consistent with a pelagic sediment sequence deposited on the oceanic crust of the Pacific plate and thrust under the prism sediments in the hanging wall. Thus, the sheared clay interval at 821.5–822.5 mbsf is interpreted as the plate boundary décollement zone between the subducting Pacific plate and the overlying prism of accreted sediment. It is noteworthy that the scaly clay décollement zone is more similar to the décollement zones in Costa Rica (e.g., Kimura, Silver, Blum, et al., 1997; Vannucchi and Tobin, 2000) and considerably thinner than the few tens of meters thick décollement zones in Nankai and Barbados (Maltman et al., 1997; Wallace et al., 2003; Kinoshita et al., 2008).

The brown silty clayey mudstone of lithologic Unit 5 displays progressively less deformation downward to a relatively undisturbed state at the basal contact with Unit 6. The unit is relatively homogeneous and bedding orientation is not clear on the core surface, possibly due to extensive bioturbation indicated in X-ray CT images. However, the sedimentary contact at the base of this unit dips 7°, similar to the few observed stratigraphic contacts within the unit. The unit is traversed by shear fractures and locally dark bands. These brittle deformation features are observed in the cut surface as well as in CT images. Located near the top of the unit are discrete zones of particularly high fracture density, and incipient scaly fabrics may be indicated by

intersecting fracture networks in zones <0.10 m thick. Shear surfaces within this unit, particularly near the base, dip between 31° and 62°, averaging about 45°.

The primary structural features in Units 6 and 7 are bedding surfaces in the clays that on average dip 6° ± 2° and three natural faults dipping 14°, 55°, and 78°. Other apparent faults probably result from drilling-induced damage, as they are bounded by significant amounts of soft, structureless, intruded clay. Overall, intact lamination in Unit 6 indicates that very little structural deformation or bioturbation affected these units of the underthrust sediments.

Biostratigraphy

Although samples were collected for analysis during the expedition, the actual analysis will be performed by a shore-based specialist. Results will be provided in the Expedition 343/343T *Proceedings* volume as an appendix or data report.

Geochemistry

Interstitial water geochemistry and headspace sampling from cores collected during the expedition were processed aboard the D/V *Chikyu*. Interstitial water samples were collected from 12 cores. Interstitial water samples showed evidence of a sulfate-bearing fluid reservoir at depth, which on the basis of the condition of the intact whole-round sections sampled, is unlikely to be from drilling-induced contamination. Chlorinity and bromide also decreased with depth, consistent with the presence of a reservoir of deeper fresher fluids.

Gas chemistry, particularly the presence of varying H_2 concentrations, may reflect mechanochemical production of H_2 during high-velocity frictional sliding and sediment disruption as would be expected for the Tohoku earthquake. Although the sampled interval is not complete and is therefore missing some key zones, the presence of a sudden sharp increase in H_2 concentration in Section 343-C0019E-5R-1 suggests the presence of a recently activated fault. Below this location, methane concentrations decrease with depth (Section 20R-2), being 2–3 orders of magnitude below the previous core; this also suggests that methane concentrations have been dissipated through subseafloor fluid flow and supports the presence of a deeper reservoir of fluids.

Microbiology

Twelve whole-round core samples were taken from various depths in Hole C0019E, and sampling procedures were completed within 60 min of the core arriving on deck.

Fixed samples were stored at –80°C for later DNA/RNA analyses. Results of the contamination tests showed that perfluorocarbon (PFC), which was added to the drilling mud, was present in the exterior portions of the whole-round samples. Also, some PFC contamination was present in the interior portions of Cores 343-C0019E-5R, 7R, 8R, 15R, and 20R but not inside of Cores 4R, 12R, and 19R. Microbiological and interstitial water data will be carefully evaluated to assess the degree of possible contamination from drilling mud and seawater.

Physical properties

Bulk density of core samples determined from moisture and density (MAD) measurements and from gamma ray attenuation measured by the whole-round multisensor core logger (MSCL-W) compare favorably. The density values generally increase with depth as expected for mechanical consolidation. The discrete samples taken from the 820 fault (Unit 4) have bulk density of 1.98 g/cm^3, whereas in the clay-rich zone just below the fault, bulk density values range from 1.76 to 2.03 g/cm^3. Porosity determined from MAD measurements decrease with depth from 55.3%–68.7% at shallow levels to ~45%–50% in the vicinity of the 720 and 820 faults. The lowest values are found in the immediate vicinity the 720 fault zone, compatible with shear-enhanced compaction.

Overall, resistivity of discrete samples from lithologic Unit 1 and into Unit 3 increases with depth but is lowered locally, possibly from the presence of ash layers. Resistivity markedly increases from the lower part of Unit 3 into Unit 4. In Units 5 and 7 from 826 to 836 mbsf, below Unit 4, resistivity is again significantly lower. Resistivity is high within the chert of Unit 7.

Qualitatively consistent with logging data, natural gamma radiation (NGR) data from the MSCL-W measured on whole rounds indicate the NGR magnitude in Unit 4 is about twice that in units above, consistent with a significant increase in the clay fraction from Unit 3 to Unit 4. NGR decreases progressively from Unit 4 downward, indicating a gradual decrease in clay content in Units 5 and 6.

P-wave velocity measured on unconfined discrete samples ranges from 1400 to 3300 m/s, but there is a clear trend of increasing velocity with depth. There is a decrease in the velocity measured on samples from lithologic Unit 5, below the 820 fault zone. A maximum velocity of ~3272 m/s occurs in the cherts of Unit 7. *P*-wave velocity has an inverse relationship with porosity, with the majority of samples following an approximately linear trend except for the chert, which has a much higher velocity. On

five select cubic samples, both *P*- and *S*-wave velocities were measured in multiple directions under stepwise increasing and decreasing confining pressure to determine pressure dependence and anisotropy. These measurements are useful for determining seismic properties at in situ pressures, as well as for inferring properties of similar sediments at greater depths in the wedge.

Thermal conductivity was measured on the working half of core sections at 45 discrete locations; the mean of all measurements is 1.139 W/(m·K) (standard deviation = 0.118 W/[m·K]). Significant deviation from the mean occurs in Unit 1 with a mean of 0.874 W/(m·K) (standard deviation = 0.0141 W/[m·K], n = 2), in Unit 6 with a mean value of 1.086 W/(m·K) (standard deviation = 0.0870 W/[m·K], n = 3), and in the chert of Unit 7 with a very high value of 1.622 W/(m·K) due to its high density and silica content.

Unconfined compressive strength (UCS) was determined for nine minicores from various depths. In general, UCS increases downhole, with locally low strength values exhibited by samples that may represent major faults or shear zones. In the lower portion of Unit 3 (below 800 mbsf), UCS is 6.4–7.6 MPa, but Unit 4 from the 820 fault zone immediately below shows lower strengths of 3.4 and 4.7 MPa. A chert sample from Unit 7 was the strongest tested, with a minimum UCS of 65.3 MPa.

Core-Log-Seismic integration

Logging units based on resistivity and gamma ray response, structural units based on bedding and fracture features in image logs, lithologic units determined from visual core description of the cores, and seismic units identified in seismic reflection profiles are integrated to develop a unified interpretation of the geology and geophysics of the drill site (Fig. **F10**). Unfortunately, core was acquired from only a portion of the entire drilled section, albeit from critically important sections, so, where possible, core samples were used to ground-truth lithologic interpretations of the logging data. Similarly, the limited suite of logging tools did not provide multiple independent measures of rock properties such as velocity, density, and porosity. Accordingly, to quantify density and seismic velocity, we determined formation factor from the resistivity logs, calculated porosity using Archie's law, and used direct measurement of discrete samples from core to constrain Archie's law. In addition, MSCL-W data were used as an intermediate step for correlation of discrete measurements from core and log data. Finally, to integrate core and log data with seismic data, a synthetic seismic trace was created for Hole C0019B. A wavelet was extracted from seismic Line HD33B, and the reflectivity series were calculated using density and velocity logs determined

from resistivity-based porosity with some adjustment of the velocity model based on crosscorrelation of seismic data and the synthetic seismic trace.

The logging units, based on gamma ray and resistivity response, compare favorably with lithologic units identified through core analysis, particularly at the base of the borehole where contrasts in lithology and geophysical response are most dramatic (Fig. **F10**). The boundary between logging Units II and III, structural Domains 2 and 3, and lithologic Units 3 and 4 correlate exactly. The changes observed across this boundary, specifically the abrupt change in bedding dip seen in image logs and core, the increase in clay content of core samples and concomitant increase in gamma ray, and the presence of the fault rocks that make up lithologic Unit 4 point to this boundary as a significant fault contact. The similarity of the lithologic units seen in core below the boundary with strata deposited on the Pacific plate (Shipboard Scientific Party, 1980b) suggests this is the plate boundary interface. Furthermore, the fact that observations of both the core samples and image logs indicate that the entire sediment section above the boundary is variably, often steeply dipping and fractured is consistent with it comprising a shortened and accreted sequence of strata.

Above the plate boundary interface and within the frontal prism, the logging unit boundaries, structural domain boundaries, and lithologic boundaries do not correlate well. Boundaries demarcated on the basis of changes in stress indicated by borehole breakout patterns also do not correlate. Moreover, the entire prism appears relatively transparent in seismic profiles. This likely reflects both the presence of inclined and faulted bedding and the relatively uniform properties of the sediment. Although the spot cores taken at 176.5–186.0 and 648.0–660.5 mbsf are considered to represent different lithologic units, both of these sections, as well as core from deeper intervals in the prism (688.5–729.0 and 770–821.5 mbsf), are mudstones composed predominantly of terrigenous silt and clay with varying amounts of vitric ash and biogenic silica. The subtle cyclicity in gamma ray and resistivity log response with depth in the prism may result from stacking packages of sediment by thrust and reverse faulting. The apparent gradual decrease in porosity with depth from progressive consolidation interrupted by stepwise increases in porosity from faulting would be is consistent with such a structural interpretation. Given the variable but dominantly steep eastward dip of the sediment throughout most of the prism, even relatively small displacement on contractional faults would lead to significant repetition of strata as seen in a vertical borehole.

A correlation exists between abrupt changes or discontinuities in different signals at a couple of different locations in the prism. For example, at ~140 mbsf, an abrupt reversal in the progressive change in borehole breakout orientation correlates with a sharp change in bedding from moderate dips to very shallow dips, which likely reflects a fault contact. Another marked change in borehole breakout distribution occurs at ~550 mbsf, and this appears to correlate with a local low gamma ray response. The 720 fault identified on the basis of image logs and resistivity curves correlates with a fault zone in core samples and an abrupt change in bedding dip.

Regional seismic images display three prominent seismic units below the lower slope of the Japan Trench where Site C0019 boreholes were drilled (Fig. **F10**). Uppermost seismic Unit 1 is wedge-shaped with an acoustically chaotic character and without continuous reflectors and corresponds to the frontal prism. Seismic Unit 2 consists of a relatively thin section of fairly continuous subhorizontal reflectors located below Unit 1 and above Unit 3. Lowermost seismic Unit 3 is the acoustic basement likely corresponding to oceanic igneous basement. Generation of the synthetic seismic trace based on resistivity logs, discrete core sample measurements of density and seismic velocity, and correlation with the seismic profile through the drill site allows location of the plate boundary fault in the seismic profile.

The synthetic seismic trace shows five possibly significant reflectors at the seafloor and at 70, 269, 368, and 839 mbsf. The middle three reflectors on the synthetic trace, at 70, 269, and 358 mbsf, fall within chaotic seismic Unit 1. Coherent reflectors within this unit are rare and, where present, are often masked by steeply dipping noise, making confident correlation within the unit difficult. Moreover, bedding at these depths in the borehole dip moderately to steeply and are thus unlikely to be apparent in seismic sections. The lowermost strong reflector on the synthetic trace falls within bedded seismic Unit 2. After crosscorrelation-based alignment with the strong reflectors at the base of the borehole, the synthetic reflector at 839 mbsf correlates best with the first strong reflector of the bedded unit at 9994 ms two-way traveltime. In the borehole, the plate boundary décollement occurs at ~820 mbsf, about 20 m shallower than the prominent reflector.

Stratigraphic control on the location of plate boundary décollements has been proposed in the past on the basis of well log and seismic data from other subduction zones (e.g., Wallace et al., 2003). Here, the décollement occurs within a thick clay-rich layer. If this represents stratigraphic control on the location of the décollement, then

the position of the plate boundary interface across the region may be inferred from seismic data.

Preliminary scientific assessment

Objective 1: identify and sample the fault that ruptured during the Tohoku earthquake

The primary scientific motivation for this expedition was to gather time-sensitive information on the stress state, chemical processes, and energetics of the Tohoku earthquake rupture at the toe of the prism. A prerequisite to achieving these goals was to locate, sample, and instrument the fault that slipped during the Tohoku earthquake. To this end, a major accomplishment of the expedition was the successful completion of three holes at Site C0019 (JFAST-3) that reached the depth of the regionally distinct seismic reflectors generally interpreted as the top of the igneous basement of the subducting Pacific plate (e.g., Tsuru et al., 2002; Kodaira et al., 2012). After the completion of the LWD/MWD hole to the target depth, we confidently assumed we had drilled across the zone of the Tohoku earthquake rupture as well as across the plate boundary interface. Moreover, contrary to expectations prior to drilling, borehole stability was not a significant issue at any depth in the hole. Thus, we concluded that hole conditions would not prevent installation of a temperature measurement observatory and that from temperature measurements we could verify the location of the earthquake rupture, provided we could identify, locate, and instrument the fault(s).

The original operations plan to use LWD/MWD data to locate the fault zone that was ruptured during the Tohoku earthquake required an extremely quick analysis that, in hindsight, was overly optimistic. As a result of operational delays, however, we had additional time to process and analyze the logging data more completely. Thus, we were able to confidently identify two significant fault targets for instrumentation and coring. The shallower fault target, the 720 fault, appeared as a meter-thick, highly conductive layer within a zone possibly tens of meters thick containing variably dipping sediment cut by conductive and resistive fractures. This feature seemed to match expectations for an earthquake rupture zone (i.e., a localized shear zone), possibly composed of gouge, within a broader zone of fractured and brecciated sediment (e.g., Sibson, 2003; Vannucchi and Tobin, 2000). However, the findings of no apparent change in lithology, bedding orientation, or borehole breakout patterns across the zone does not support the interpretation of a large displacement fault. The deeper

fault target, the 820 fault, was identified on the basis of an apparent marked change in structure and lithology. Specifically, image log data showed the prism comprises a northeastward striking but variably dipping stack of sediments, as would be produced by folding and faulting during northwestward convergence and accretion. Steeply dipping beds near the base of the prism are truncated and in sharp contact with a very shallow dipping, concordant sequence of interbedded sediments that appeared to coincide with the regional seismic reflector associated with the top of the oceanic crust of the Pacific plate. The resistivity and gamma ray log response of the sediments below the contact indicate distinct lithostratigraphic units, unlike the log response of the sediments in the prism above. Overall, the abrupt structural and lithologic change across the contact is strongly suggestive of a plate boundary décollement between a deformed prism above and subducting oceanic crust below. However, the contact itself is unremarkable in image logs and displays little evidence of an associated fractured or brecciated zone with lowered resistivity as might be expected for a plate boundary fault zone recently ruptured by a great earthquake.

The two faults identified on the basis of LWD/MWD data were treated as equally important targets in planning the temperature measurement observatory and the coring hole. Accordingly, the location and spacing of the MTLs in the observatory was modified to acquire adequate measurement of temperature transients near either of the targets. The installation of the temperature measurement observatory was prioritized up to the point in time the underwater television (UWTV) cable failed and could not be repaired. Coring operations commenced once it was clear the observatory could not be installed, but the remaining time was very limited. Accordingly, we devised a plan for coring only across each of the primary targets and that included taking very short cores over the several meters spanning the fault targets.

Shipboard observations of the samples collected from the second coring hole confirmed the inferences drawn from the LWD/MWD data set and clarified the nature of the targeted fault features. All cores taken from the prism (i.e., from depths shallower than the 820 fault) consist of clayey to silty mudstones comprising terrigenous silt and clay, vitric ash, and biogenic silica. Measurements of bedding orientation in cores from the prism show locally variable dip, as well as the existence of discrete changes in dip as might occur across faults. The entire suite of core samples taken from the prism is variably dissected by dark shear bands and open fractures that are tectonic in origin or other tectonic discontinuities that were opened by drilling. A prominent fractured and brecciated zone extends from 719 mbsf to deeper than 725 mbsf and bounds the prominent low-resistivity 720 fault. Several core samples from the frac-

tured and brecciated zone contain minor faults, the largest and most prominent of which is a high-angle reverse fault that occurs at the same depth as the low-resistivity feature in the image logs. Although no geochemical anomaly was identified in the fractured and brecciated zone near the 720 fault, a local H_2 and chlorinity anomaly was documented near 700 mbsf. The increase in H_2 may have been generated by recent faulting, and the local reduction in chlorinity could reflect focused flow of fluids from a deeper source.

The data from core samples support the overall interpretation made on the basis of logging data that the 820 fault is the plate boundary décollement between the deformed sediments of the prism above and the basal sedimentary strata and igneous oceanic crust of the incoming Pacific plate below. Core samples clearly document an abrupt and marked change in bedding dip at the 820 fault; although it is not at all apparent in the logging data, a zone of highly sheared clay is present below the contact and was sampled by the coring. The zone is between 1 and 5 m in thickness and is characterized by a scaly fabric that, locally, is penetrative to the millimeter scale. Immediately above and below the sheared layer, visual and X-ray CT observations document that the deformation intensity of the sediment decreases rapidly with distance from the layer in a manner consistent with typical fault-related damage patterns. Lithologically, the multicolored clay layers and chert in the footwall of the 820 fault closely match the descriptions of the pelagic sediments recovered from the base of the drill hole on the Pacific plate east of the Japan Trench (Leg 56 Site 436; Shipboard Scientific Party, 1980b) and contrast markedly from the terrigenous sediments in the hanging wall of the décollement. The coincident lithologic and bedding discontinuity across the layer, the presence of deformed sediments bounding the layer, and the shear fabric of the clay in the layer are all compatible with the interpretation of a large displacement, plate boundary décollement.

The location of the décollement coincides with the uppermost reflector of the several distinct and parallel reflectors that demarcate the top of the subducting oceanic plate. As shown by the in-line seismic profile that passes through the drill site, these reflectors are continuous for ~1 km to the east-southeast and several kilometers to the west-northwest. The cross-line seismic profile that passes through the drill site indicates the reflectors are continuous several kilometers along strike to the north-northeast and south-southwest. Approximately 1 km in-line to the east-southeast, the basement is down-dropped along normal faults to form a prominent sediment-filled graben that spans the axis of the trench. A distinct reflector continues from the reflectors at the top of the horst below the drill site to the east and into the sediment fill of the

graben (Fig. F2). The seismic character of this reflector is consistent with the general structure of the décollement documented at the drill site (i.e., a hanging wall characterized as chaotic and seismically transparent and a footwall consisting of subhorizontal and conformable seismic reflectors representing the bedded sediments and underlying igneous basement of the subducting plate). The reflector continues from the horst into the graben and cuts some sediment layers in the footwall, and thus defines the base of the displaced and thickened prism (also see Kodaira et al., 2012). The seismic data support the simple interpretation that the prism extends some 3 km east from the drill site to the axis of the trench. A first-order palispastic reconstruction of the prism, assuming constant area balancing, implies the displacement on the décollement at the drill site is on the order of 3 km. Although the deformation associated with the décollement is much more localized than that seen at other subduction décollements (e.g., Nankai, Barbados), the structure and fabric of the décollement at the drill site is compatible with displacements of this magnitude. Thus it is expected that the décollement at the drill site is likely continuous with the deeper portions of the plate boundary interface tens of kilometers downdip. A plate boundary décollement of this size and position is hypothesized as the locus of tectonic displacement of the subducting plate in the geologic past, as well as during the recent rupture that propagated to the trench during the Tohoku event.

After analysis of core samples from both the 720 and 820 fault zones, the design of the MTL autonomous observatory was modified to primarily target the 820 fault using a dense array of sensors; however, sensor placement to characterize a possible temperature anomaly at the 720 fault has been retained. In addition, some sensors are programed to acquire data at higher frequencies at the time of scheduled retrieval in order to directly measure a temperature profile of the entire hole as the string is pulled out. Thus, the observatory is expected to provide valuable data when the sensor string is later retrieved, which is scheduled for October 2012 or February 2013. The observatory data will document the spatial and transient character of the temperature distribution in the lower reaches of the borehole. These results will not only allow confirmation that the rupture occurred at the décollement but will also lead to a robust estimate of the frictional heat generated during the dynamic slip of the Tohoku earthquake. The determination of total heat can constrain models used to estimate the dynamic shear strength of the fault and infer the magnitude of the coefficient of friction.

Objective 2: what was the stress state on the fault that controls rupture during the earthquake and was the stress completely released?

The most significant goal of this rapid response drilling project is to determine the dynamic frictional stress. Data from the measurement of the time decaying temperature anomaly associated with the earthquake slip will be used to estimate the frictional heat produced at the time of the earthquake, which can be used to infer the level of dynamic friction (e.g., Brodsky et al., 2009; Fulton et al., 2010). Measurements of current stress (i.e., postearthquake slip) also can be used to explore different models to explain how dynamic slip occurred and the degree to which stress was released. The in situ stress will also be determined through the use of LWD image logs to characterize borehole deformation (e.g., Zoback et al., 2003) and measurements of anelastic strain recovery (ASR) of core samples (e.g., Byrne et al., 2009). Several samples were collected for ASR, and these time-sensitive measurements were begun during this expedition. Measurements and analysis will be completed within several months of the end of the expedition and, if successful, could provide true 3-D determination of in situ stress in the prism.

The borehole breakouts evident in image logs from the LWD hole indicate several different in situ stress domains within the prism. At depths less than ~200 mbsf, the maximum horizontal compressive stress (S_{Hmax}) systematically varies from approximately parallel to the convergence direction to perpendicular (at 140 mbsf) and back toward parallelism again with greater depth. At intermediate depths (200–537 mbsf), S_{Hmax} orientation is variable and nonsystematic. At deeper levels in the prism (537–820 mbsf), S_{Hmax} displays a single preferred orientation ~20° clockwise from the convergence direction. Faults and bedding are variable in dip magnitude, but faults and bedding at all depths in the prism show a preferred northeast strike direction reflecting horizontal contraction and local extension approximately parallel to the plate convergence direction. That S_{Hmax} varies with depth in the prism likely indicates a postearthquake stress state in the prism in which S_{Hmax} is similar in magnitude to S_{hmin} except possibly in the very basal part of the prism. The variation at shallow depths can be understood as a result of reduction in the magnitude of the horizontal stress in the direction of slip during the earthquake. If the magnitude of maximum horizontal stress is reduced to values similar to the minimum horizontal stress, then borehole breakout directions will reflect local perturbations and appear highly variable or they may change systematically with depth because of variation in mechanical properties or the presence of other tectonic discontinuities. Thus, these preliminary data on S_{Hmax} directions are consistent with a reduction of shear stress on the megathrust dur-

ing the Tohoku earthquake, but further analysis is necessary to infer the magnitude of stress changes.

Objective 3: what are the characteristics of large earthquakes in the fault zone, and how can we distinguish present and past events in fault zone cores?

Success in recovering ~1 m of core from the high–shear strain zone and neighboring sediments from the plate boundary décollement provides material for shore-based mechanical and physical properties testing, as well as for geochemical, mineralogical, and microstructural analyses. Physical properties testing, particularly for thermal and fluid-flow properties, are important for constraining models of thermal-mechanical-hydrological processes important to the seismic cycle, modeling thermal transients in order to infer the dynamic strength of the Tohoku earthquake fault, and determining stress state of the prism over the seismic cycle. Several shore-based studies of frictional properties of intrafault materials as a function of slip rate, pressure, temperature, and fluids are planned; this information will feed into mechanical analyses of seismic faulting. In addition, three special interest structural whole-round samples taken from the sheared clay of the décollement, as well as two other structural whole-rounds capturing secondary faults, will provide material for coordinated nondestructive and destructive investigations of structure, chemistry, and mineralogy of the faulted sediments. These studies and those of geochemistry and other physical properties will be used to search for signatures of seismic slip and investigate processes of dynamic slip during large earthquakes.

Expedition 343 operations

Shimizu, Japan, port call

Loading for Expedition 343 began on 25 March 2012 at Shimizu, Japan. A “prespud” meeting was held aboard the *Chikyu,* with representatives from Center for Deep Earth Exploration (CDEX), Marine Works Japan, Mantle Quest Japan, and the Expedition 343 Science party on 31 March 2012. The *Chikyu* departed Shimizu at 1630 h on 1 April en route to Site C0019 (proposed Site JFAST-3).

Transit to Site C0019

During transit to Site C0019, the *Chikyu* engaged in a series of system integration tests with the dual elevator system (DES) and began building up drill pipe stands and casing running tools for the 20 inch wellhead. The *Chikyu* arrived on site at 0800 h on 3 April 2012. However, extreme winds (30 m/s, maximum gusts near 40 m/s) necessitated putting the vessel into auto heading mode and entering wait on weather (WOW) while weather conditions remained poor. The *Chikyu* continued to WOW until the morning of 5 April, when transponders were dropped and continued to make up dynamic positioning. The UWTV cable was rigged up in the moonpool for a free-fall test on 6 April and required troubleshooting the winch and software issues affecting deployment. While the UWTV was undergoing troubleshooting, the jetting and running bottom-hole assembly (BHA) for the MTL observatory was being rigged up and tested. Testing for the UWTV continued over several days, working to solve twisting and kinking issues. Eventually, the *Chikyu* needed to be moved to deeper water (7500 m) to fully unwind the weighted UWTV cable. Problem solving focused on eliminating unwanted rotation in the cable, which could result in wrapping and snapping the UWTV cable on the drill string while deployed near the seafloor. Finally, on 13 April, the *Chikyu* moved to the site location and prepared the guide horn and running tool for the 20 inch casing. All the holes surveyed and drilled at Site C0019 were along a transect running along strike at ~10 m intervals (Fig. **F3**).

Hole C0019A

Initial operations began with running the 20 inch casing with a 30 inch outside diameter guide funnel into the water at 1800 h, reaching 2415 m drilling depth below rig floor (DRF) at 2400 h. Once the BHA reached 4074 m DRF, the DES was installed and tested in preparation for running deeper. However, several problems with the DES operation were discovered, delaying jetting in Hole C0019A. Preparations for running the UWTV were made but then postponed because of 14 h of WOW (waves exceeding operational criteria). After WOW, the UWTV dove to the wellhead housing at 4677 m DRF. While running to the seafloor, the DES and UWTV continued to experience problems during operation. A seabed survey started on 17 April at 1945 h, taking advantage of the weather and close proximity of the coring hole and the LWD hole. Once the survey was completed, the *Chikyu* returned to the LWD hole position to spud in the 20 inch casing. After troubleshooting the DES again, jetting in Hole C0019A (37°56.3367′N, 143°54.8100′E) began on 18 April at 0745 h. The jetting was successful to 28.0 mbsf, but the running tool would not release. Many attempts were

made to release the running tool, but all were unsuccessful. It was decided to recover the running tool dart with the wireline winch, which eventually succeeded by 2030 h. Investigation showed no apparent issues with the dart, so the running tool dart was rerun with a new shear pin. The tool still refused to part from the wellhead, so attempts were made to jar down nine times. Attempts at raising pressure and repeating dart landings were equally unsuccessful, while continuous observation via the UWTV showed no apparent mechanical irregularities that might account for the stuck casing. Upon retrieval, the X Barrel Retrieving Tool showed no pin shear. Ultimately, the decision was made on 19 April to pull the casing and running tool out of the hole and return them to the rig floor for inspection. On 20 April, the running tool and wellhead were laid down for careful inspection and testing of the running tool. During this time, the *Chikyu* moved to drop a new seafloor transponder to replace a malfunctioning one. Since the jet-in failed, it was decided to move on and begin LWD drilling at a new hole.

Hole C0019B

Preparations began to assemble the LWD BHA to drill the logging hole while the casing and casing running tool were inspected. On 21 April, the LWD tools were made up and run in for a shallow-water test. Unfortunately, a first shallow communication and function test at the sea surface revealed that the proVISION tool was not functioning properly. After some unsuccessful attempts at repair, the tool was removed, and then the 8½ inch LWD BHA including geoVISION, arcVISION, and MWD (TeleScope) tools was run. Subsequent shallow tests of the MWD pulse telemetry were conducted at water depths of 1988.7, 3872.4, and 5985.0 m. Spud-in of Hole C0019B was achieved at 0011 h on 23 April, followed by jetting in with an initial surface pump rate of 150–500 gallons per minute (gpm). About 1 h later the spud-in pumping rate was increased and the MWD mud-pulse transmission was confirmed. At around 0916 h the bit passed 7049.5 meters below sea level (mbsl). This is the deepest total length from the sea level in the history of scientific ocean drilling. After continuous drilling and real-time monitoring to 576.0 mbsf, the drill string was pulled up due to WOW on 24 April. Drilling operation was resumed from 576.0 mbsf at 2400 h on 24 April. In the evening of 25 April, the largest changes in resistivity and NGR were observed at the interval of about 820–840 mbsf. The large changes in the logging parameters were interpreted that the LWD had reached hard chert layer, which was the designated target formation. At 2143 h on 25 April, the rate of penetration had dropped to nearly zero and the decision was made to stop drilling. The borehole reached a final

depth of 850.5 mbsf (7740 mbsl). This extends the world record for total length of drill pipe below sea level, which was set 2 days earlier. Repeated measurements at three designated 50 m intervals were conducted while pulling out of the borehole. By the end of the day of 25 April the LWD assembly was out of the borehole, all LWD tools were recovered on the rig floor at 1200 h on 27 April, and all memory data were successfully downloaded.

Hole C0019C

Preparations for the wellhead installation in Hole C0019C began on 28 April with the make-up and running of the 20 inch casing and running tool BHA. The wellhead and running tool BHA were run into the water from 0215 h and had reached 4084 m DRF by 1415 h. To prevent problems with the inner lining of the drill pipe from fouling the running dart landing, the pipe was flushed with 1000 gpm of seawater at 1000, 2000, 3000, and 4000 m. The UWTV was installed and run in the hole from 2000 h and underwent a function check at 180 m. Communication checks failed to contact the minibeacon, and a phase of troubleshooting the issue began. The drill pipe continued to be run in, in conjunction with the UWTV, until the seafloor was tagged at 0815 h on 29 April. Jetting in the 20 inch casing began in Hole C0019C at 1500 h, confirming the seafloor depth at 6928.5 m DRF, stopping only when the casing had reached 29 mbsf. Upon starting to pick up the core barrel retrieving tool (CBRT), it was found that the core line winch counter was malfunctioning, so it was run with a calculated pay out. Circulation to clear out Hi-Vis mud began, and then the CBRT with dart was run to 6721 m DRF without pumping. Closing and pumping at 20, 40, and 60 strokes per minute (spm) began when the CBRT suddenly released the wellhead; recovery of the CBRT and dart showed that the dart broke in two within the drill pipe. The UWTV and drill pipe were pulled up to 4100 m DRF, checking the minibeacon signal on the UWTV every 1000 m with no response. The UWTV was recovered to the surface by 1415 h on 30 April, while the running tool BHA was recovered and laid down on 1 May.

The LWD assembly was made up in preparation for reentry into the wellhead of Hole C0019C on 1 May. Just as for Hole C0019B, the LWD tools included the geoVISION, arcVISION, and MWD (TeleScope). Following the standard procedure, the tools were assembled, and shallow communication and function tests were conducted on the surface and at water depths of 320, 2014, and 3917 m. On 2 May, due to bad weather, the drill string was brought up to ~3000 m and secured for riding out the rough seas. Following 2 days of WOW, operations resumed, running the LWD assembly with

UWTV on 5 May. Adjusting vessel position, the attempt to reenter the wellhead was successful at 0000 h on 5 May. The LWD assembly was continuously run into Hole C0019C; however, there was an engineering problem at 1400 h on 6 May with a loss of the BHA at ~120 mbsf. The cause of the problem is being examined. Analysis of LWD data showed that the disconnection of the BHA was not a result of any abnormal conditions of the borehole or the response of the formations being drilled. Once the pipe was returned to the ship on 7 May, the engineering staff determined it was a mechanical failure of one section of the drill pipe. The loss of the BHA inside the wellhead necessitated abandoning this hole and starting preparation for jetting a new wellhead in Hole C0019D.

Hole C0019D

Preparation for jetting a new wellhead in Hole C0019D began at 1700 h on 7 May once the remaining sections of the LWD BHA had been recovered and examined on the rig floor. On 8 May, the jetting BHA and running tool were made up and run into the water, reaching 5030 m DRF by 1000 h. The seafloor was reached by 0500 h on 9 May, and Hole C0019D was tagged at 0630 h at 6929.5 m DRF. Jetting in operations began at 0945 h, when the seabed was noted as being 6926 m DRF, a 3.5 m difference! The wellhead was jetted in to 27.5 mbsf by 1245 h, when operations to release the running tool began. Several issues were noted, particularly that the tool would not release, even after confirming landing of the dart several times. The drillers made multiple attempts over the next few hours, finally noting, by visual UWTV confirmation, that the tool had released at 2000 h. Preparations for drilling ahead began with the UWTV recovery, when the video feed from the UWTV was lost. Attempts to recover visual communications failed, so the UWTV was recovered on deck to examine it more closely. Finally, at 1000 h on 10 May, the UWTV was recovered on the working cart above the moonpool so that troubleshooting could begin. Meanwhile the jetting BHA was recovered on deck, laying down at 2130 h. The umbilical cable for the UWTV was found to have one more cut fiber-optic line and two short circuits in the power lines, all close to the spool connection. A quick consultation among the Co-Chief Scientists, Operations Superintendents (OSI), Offshore Installation Managers (OIM), and Expedition Project Managers (EPM) concluded that since the problem could not be fixed rapidly, coring operations would begin immediately.

Hole C0019E

The decision was made on 10 May to proceed with a blind spud of Hole C0019E with the coring BHA without use of the UWTV. The location was selected with two considerations in mind: (1) it was close to Hole C0019B (10 m south of Hole C0019B), where the LWD data could guide and identify coring key target intervals, and (2) it was far enough away to minimize the possibility that the holes would intersect at depth. The RCB coring BHA was made up and run in the hole on the morning of 11 May, reaching 4000 m DRF by 1845 h. Sea conditions necessitated WOW, which continued until 0600 h on 12 May. There were several more short WOW periods during 12 May, mainly due to maximum wave heights exceeding operational parameters. The seafloor was reached on 13 May, when the center bit was dropped for washing down and tagging the seafloor. The seafloor depth (6918 m DRF) was estimated from drilling parameters and the proximity of Hole C0019E to the LWD Hole C0019B. A test core was performed from 176.5–186 mbsf and recovered on deck on 14 May at 0752 h. It was decided to drill ahead before beginning the next series of coring operations, which began on 16 May at 648 mbsf. Cores 343-C0019E-2R and 3R were recovered, and then we drilled ahead to 680 mbsf. From this point, we cored continuously until reaching 729 mbsf on 19 May, when a consultation among the OSI, OIM, Co-Chief Scientists, and EPM decided that with the limited time left to the expedition, we would drill ahead to 770 mbsf before coring resumed. The drill ahead target was reached on 19 May, with the first core (343-C0019E-10R) of the second coring run on deck at 2359 h. It was decided to core ahead until the end of 22 May so that we would have the best chance of recovering the next identified presumed fault zone at 820 mbsf. Coring operations finished at 844.5 mbsf at 1640 h on 22 May, with the recovery of Core 343-C0019E-21R, a short chert section of 0.5 m, after a drilling advance of 8 m. A deplugger assembly containing three MTL sensors was dropped, and then pulling out of the hole operations commenced. The BHA was recovered on deck 0400 h on 24 May, and the ship began moving 30 nmi west of Site C0019 to reach the helicopter rendezvous point from 0445 h.

Expedition 343 end

Expedition 343 ended at sea on 24 May 2012, with the helicopter transfer (in three flights) of the science party to Sendai, Japan, from the *Chikyu*. In July 2012, the expedition continued as Expedition 343T in order to deploy the MTL observatory.

Expedition 343T operations

Expedition 343T operations began at sea on 5 July 2012. This expedition was a continuation of JFAST, and the goal was to deploy the MTL observatory, which failed during Expedition 343. Sensors were installed into the tubing on the rig floor on 14 July and lowering the observatory to the seafloor began that evening. The bottom of the observatory tubing entered the wellhead at ~1045 h on 16 July and was lowered into place until the casing hanger met with the seafloor wellhead at ~1730 h. Detachment of the casing running tool was completed at ~1815 h on 16 July. Recovery of the casing running tool continued until 0600 h on 17 July, after which an unsuccessful attempt was made to recover the transponders. The *Chikyu* began transit to Hachinohe Port at 1245 h, reaching the standby anchoring point at 0900 h on 18 July. The scientists disembarked via harbor boat, ending Expedition 343T at midnight on 19 July.

References

Ammon, C.J., Lay, T., Kanamori, H., and Cleveland, M., 2011. A rupture model of the 2011 off the Pacific coast of Tohoku earthquake. *Earth, Planets Space,* 63(7):693–696. **doi:10.5047/eps.2011.05.015**

Apel, E.V., Bürgmann, R., Steblov, G., Vasilenko, N., King, R., and Prytkov, A., 2006. Independent active microplate tectonics of northeast Asia from GPS velocities and block modeling. *Geophys. Res. Lett.,* 33(11):L11303. **doi:10.1029/2006GL026077**

Argus, D.F., Gordon, R.G., and DeMets, C., 2011. Geologically current motion of 56 plates relative to the no-net-rotation reference frame. *Geochem., Geophys., Geosyst.,* 12(11):Q11001. **doi:10.1029/2011GC003751**

Arthur, M.A., and Adelseck, C.G., Jr., 1980. Acknowledgments, introduction, and explanatory notes: the Japan Trench transect, Legs 56 and 57, Deep Sea Drilling Project. *In* Scientific Party, *Init. Repts. DSDP,* 56, 57 (Pt. 1): Washington, DC (U.S. Govt. Printing Office), 3–21. **doi:10.2973/dsdp.proc.5657.101.1980**

Avouac, J.-P., 2011. Earthquakes: the lessons of Tohoku-Oki. *Nature (London, U. K.),* 473(7356):300. **doi:10.1038/nature10265**

Brodsky, E.E., Ma, K.-F., Mori, J., Saffer, D.M., and the participants of the ICDP/SCEC International Workshop, 2009. Rapid response fault drilling: past, present, and future. *Sci. Drill.,* 8:66–74. **doi:10.2204/iodp.sd.8.11.2009**

Byrne, T.B., Lin, W., Tsutsumi, A., Yamamoto, Y., Lewis, J.C., Kanagawa, K., Kitamura, Y., Yamaguchi, A., and Kimura, G., 2009. Anelastic strain recovery reveals extension across SW Japan subduction zone. *Geophys. Res. Lett.,* 36(23):L23310. **doi:10.1029/2009GL040749**

Center for Deep Earth Exploration, 2012. IODP Expedition 343 drilling program. *CDEX Tech. Rep.,* 16.

DeMets, C., Gordon, R.G., and Argus, D.F., 2010. Geologically current plate motions. *Geophys. J. Int.,* 181(1):1–80. **doi:10.1111/j.1365-246X.2009.04491.x**

Fujii, Y., Satake, K., Sakai, S., Shinohara, M., and Kanazawa, T., 2011. Tsunami source of the 2011 off the Pacific coast of Tohoku earthquake. *Earth, Planets Space,* 63(7):815–820. **doi:10.5047/eps.2011.06.010**

Fujiwara, T., Kodaira, S., No, T., Kaiho, Y., Takahashi, N., and Kaneda, Y., 2011. The 2011 Tohoku-Oki earthquake: displacement reaching the trench axis. *Science,* 334(6060):1240. **doi:10.1126/science.1211554**

Fulton, P.M., Harris, R.N., Saffer, D.M., and Brodsky, E.E., 2010. Does hydrologic circulation mask frictional heat on faults after large earthquakes? *J. Geophys. Res., [Solid Earth],* 115(B9):B09402. **doi:10.1029/2009JB007103**

Hashimoto, C., Noda, A., Sagiya, T., and Matsu'ura, M., 2009. Interplate seismogenic zones along the Kuril-Japan Trench inferred from GPS data inversion. *Nat. Geosci.,* 2(2):141–144. **doi:10.1038/ngeo421**

Ide, S., Baltay, A., and Beroza, G.C., 2011. Shallow dynamic overshoot and energetic deep rupture in the 2011 Mw 9.0 Tohoku-Oki earthquake. *Science,* 332(6036):1426–1429. **doi:10.1126/science.1207020**

Ito Y., Tsuji, T., Osada, Y., Kido, M., Inazu, D., Hayashi, Y., Tsushima, H., Hino, R., and Fujimoto, H., 2011. Frontal wedge deformation near the source region of the 2011 Tohoku-Oki earthquake. *Geophys. Res. Lett.,* 38(15):L00G05. **doi:10.1029/2011GL048355**

Kanamori, H., Miyazawa, M., and Mori, J., 2006. Investigation of the earthquake sequence off Miyagi prefecture with historical seismograms. *Earth, Planets Space,* 58(12):1533–1541. **http://www.terrapub.co.jp/journals/EPS/abstract/5812/58121533.html**

Kimura, G., Silver, E.A., Blum, P., et al., 1997. *Proc. ODP, Init. Repts.,* 170: College Station, TX (Ocean Drilling Program). **doi:10.2973/odp.proc.ir.170.1997**

Kinoshita, M., Tobin, H., Moe, K.T., and the Expedition 314 Scientists, 2008. NanTroSEIZE Stage 1A: NanTroSEIZE LWD transect. *IODP Prel. Rept.,* 314. **doi:10.2204/iodp.pr.314.2008**

Kita, I., Matsuo, S., and Wakita, H., 1982. H_2 generation by reaction between H_2O and crushed rock: an experimental study on H_2 degassing from the active fault zone. J. *Geophys. Res., [Solid Earth],* 87(B13):10789–10795. **doi:10.1029/JB087iB13p10789**

Kodaira, S., No, T., Nakamura, Y., Fujiwara, T., Kaiho, Y., Miura, S., Takahashi, N., Kaneda, Y., and Taira, A., 2012. Coseismic fault rupture at the trench axis during the 2011 Tohoku-oki earthquake. *Nat. Geosci.,* 5(9):646–650. **doi:10.1038/NGEO1547**

Lin, W., Saito, S., Sanada, Y., Yamamoto, Y., Hashimoto, Y., and Kanamatsu, T., 2011. Principal horizontal stress orientations prior to the 2011 Mw 9.0 Tohoku-Oki, Japan, earthquake in its source area. *Geophys. Res. Lett.,* 38(17):L00G10. **doi:10.1029/2011GL049097**

Maltman, A., Labaume, P., and Housen, B., 1997. Structural geology of the décollement at the toe of the Barbados accretionary prism. *In* Shipley, T.H., Ogawa, Y., Blum, P., and Bahr, J.M. (Eds.), *Proc. ODP, Sci. Results,* 156: College Station, TX (Ocean Drilling Program), 279–292. **doi:10.2973/odp.proc.sr.156.037.1997**

Mori, J., Chester, F.M., Eguchi, N., and Toczko, S., 2012. Japan Trench Fast Earthquake Drilling Project (JFAST). *IODP Sci. Prosp.,* 343. **doi:10.2204/iodp.sp.343.2012**

Ozawa, S., Nishimura, T., Suito, H., Kobayashi, T., Tobita, M., and Imakiire, T., 2011. Coseismic and postseismic slip of the 2011 magnitude-9 Tohoku-Oki earthquake. *Nature (London, U. K.),* 475(7356):373–376. **doi:10.1038/nature10227**

Sacks, I.S., Suyehiro, K., Acton, G.D., et al., 2000. *Proc. ODP, Init. Repts.,* 186: College Station, TX (Ocean Drilling Program). **doi:10.2973/odp.proc.ir.186.2000**

Sato, M., Ishikawa, T., Ujihara, N., Yoshida, S., Fujita, M., Mochizuki M., and Asada, A., 2011. Displacement above the hypocenter of the 2011 Tohoku-Oki earthquake. *Science,* 332(6036):1395. **doi:10.1126/science.1207401**

Shipboard Scientific Party, 1980a. Site 434: the lower trench slope, Leg 56. *In* Scientific Party, *Init. Repts. DSDP,* 56, 57 (Pt. 1): Washington, DC (U.S. Govt. Printing Office), 355–398. **doi:10.2973/dsdp.proc.5657.106.1980**

Shipboard Scientific Party, 1980b. Site 436: Japan Trench outer rise, Leg 56. *In* Scientific Party, *Init. Repts. DSDP,* 56, 57 (Pt. 1): Washington, DC (U.S. Govt. Printing Office), 399–446. **doi:10.2973/dsdp.proc.5657.107.1980**

Sibson, R.H., 2003. Thickness of the seismic slip zone. *Bull. Seismol. Soc. Am.,* 93(3):1169–1178. **doi:10.1785/0120020061**

Simons, M., Minson, S.E., Sladen, A., Ortega, F., Jiang, J., Owen, S.E., Meng, L., Ampuero, J.-P., Wei, S., Chu, R., Helmberger, D.V., Kanamori, H., Hetland, E., Moore, A.W., and Webb, F.H., 2011. The 2011 magnitude 9.0 Tohoku-Oki earthquake: mosaicking the megathrust from seconds to centuries. *Science,* 332(6036):1421–1425. **doi:10.1126/science.1206731**

Tsuru, T., Park, J.-O., Miura, S., Kodaira, S., Kido, Y., and Hayashi, T., 2002. Along-arc structural variation of the plate boundary at the Japan Trench margin: implication of interplate coupling. *J. Geophys. Res., [Solid Earth],* 107(B12):2357. **doi:10.1029/2001JB001664**

Tsuru, T., Park, J.-O., Takahashi, N., Kodaira, S., Kido, Y., Kaneda, Y., and Kono, Y., 2000. Tectonic features of the Japan Trench convergent margin off Sanriku, northeastern Japan, revealed by multichannel seismic reflection data. *J. Geophys. Res., [Solid Earth],* 105(B7):16403–16413. **doi:10.1029/2000JB900132**

Vannucchi, P., and Tobin, H., 2000. Deformation structures and implications for fluid flow at the Costa Rica convergent margin, ODP Sites 1040 and 1043, Leg 170. *J. Struct. Geol.,* 22(8):1087–1103. **doi:10.1016/S0191-8141(00)00027-4**

von Huene, R., Klaeschen, D., Cropp, B., and Miller, J., 1994. Tectonic structure across the accretionary and erosional parts of the Japan Trench margin. *J. Geophys. Res., [Solid Earth],* 99(B11):22349–22361. **doi:10.1029/94JB01198**

von Huene, R., Ranero, C.R., and Vannucchi, P., 2004. Generic model of subduction erosion. *Geology,* 32(10):913–916. **doi:10.1130/G20563.1**

Wallace, G., Moore, J.C., and DiLeonardo, C.G., 2003. Controls on localization and densification of a modern décollement: northern Barbados accretionary prism. *Geol. Soc. Am. Bull.,* 115(3):288–297. **doi:10.1130/0016-7606(2003)115<0288:COLADO>2.0.CO;2**

Zoback, M.D., Barton, C.A., Brudy, M., Castillo, D.A., Finkbeiner, T., Grollimund, B.R., Moos, D.B., Peska, P., Ward, C.D., and Wiprut, D.J., 2003. Determination of stress orientation and magnitude in deep wells. *Int. J. Rock Mech. Min. Sci.,* 40(7–8):1049–1076. **doi:10.1016/j.ijrmms.2003.07.001**

Table T1. Expedition 343/343T coring summary.

Hole	Latitude	Longitude	Water depth (mbsl)	Cores (*N*)	Interval cored (m)	Core recovered (m)	Recovery (%)	Drilled interval (m)	Total penetration (m)	Time on site (days)
343-										
C0019E	37°56.3343′N	143°54.8084′E	6887.5	21	137	53.31	43	707.5	844.5	9
C0019A	37°56.3367′N	143°54.8100′E	6883.5	0	NA	NA	NA	28	28	3
C0019B	37°56.3033′N	143°54.7875′E	6889.5	0	LWD/MWD	LWD/MWD	LWD/MWD	850.5	850.5	21
C0019C	37°56.3033′N	143°54.7875′E	6928.5	0	NA	NA	NA	120	120	3
C0019D	37°56.3224′N	143°54.8004′E	6897.5	0	NA	NA	NA	27.5	27.5	3
		Expedition 343 totals:		21	137	53.31	43	1733.5	1870.5	39
343T-										
C0019D	37°56.3224′N	143°54.8004′E	6897.5	0	NA	NA	NA	854.8	854.8	10
		Expedition 343T totals:		0	NA	NA	NA	854.8	854.8	10
		Site C0019 totals:		21	137	53.31	43	2588.3	2725.3	49

NA = not applicable. LWD = logging while drilling, MWD = measurement while drilling.

Figure F1. A. Location map, showing the eastern coastline of Honshu, bathymetry, Tohoku earthquake epicenter (black star), and location of Expedition 343/343T Site C0019 (red star). DSDP Leg 56 Hole 434 and ODP Leg 186 Holes 1150 and 1151 (green circles) are also shown. White arrow = direction of Pacific plate convergence vector. **B.** Inset map shows orientation of in-line seismic section Line HD33B shown in Figure F2.

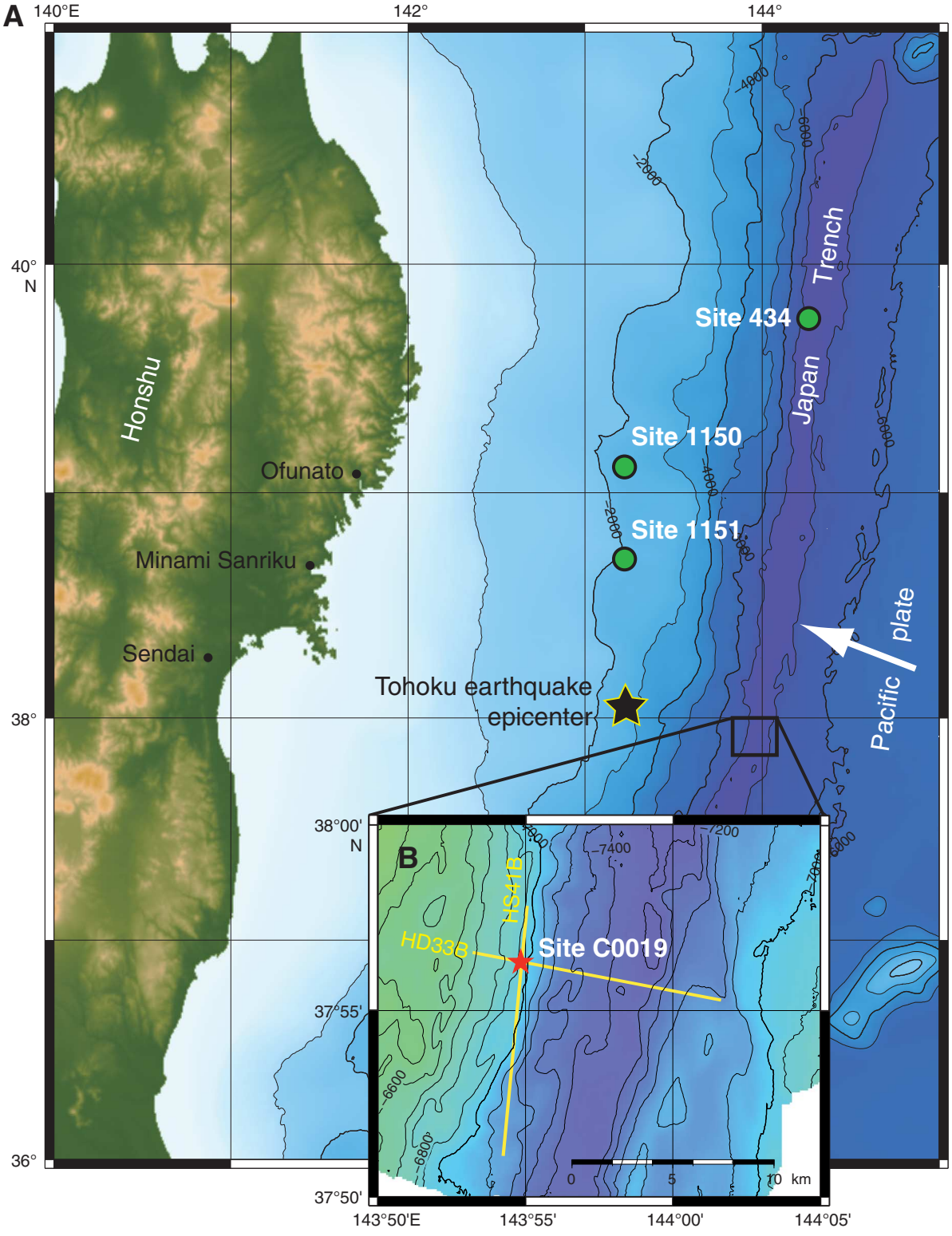

Figure F2. A portion of depth-corrected seismic Line HD33B through Site C0019. The section is partially interpreted, identifying the reflector at the top of the oceanic igneous crust of the incoming Pacific plate, top of the bedded chert, and sedimentary cover. The location of the reflector interpreted as the main décollement between the subducting Pacific plate and the deformed sediments of the overthrust frontal prism are also shown. VE = vertical exaggeration. Modified from Center for Deep Earth Exploration (2012).

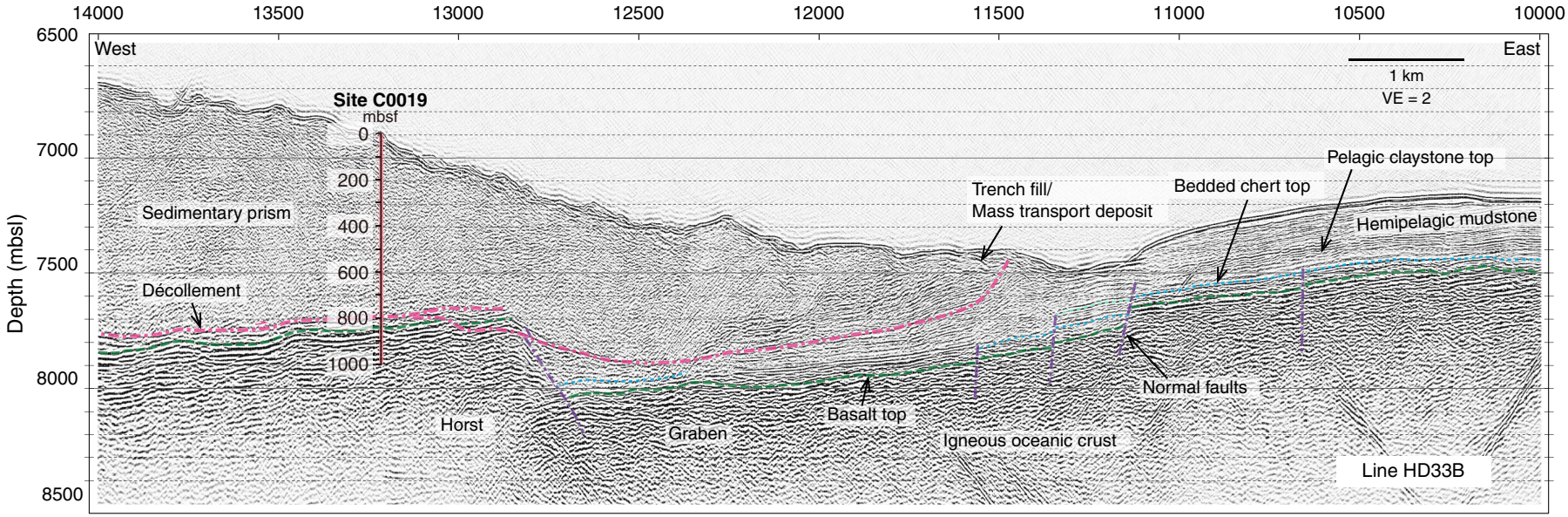

Figure F3. JFAST site map, showing the location of Holes C0019A–C0019E on a contoured base map of bathymetry.

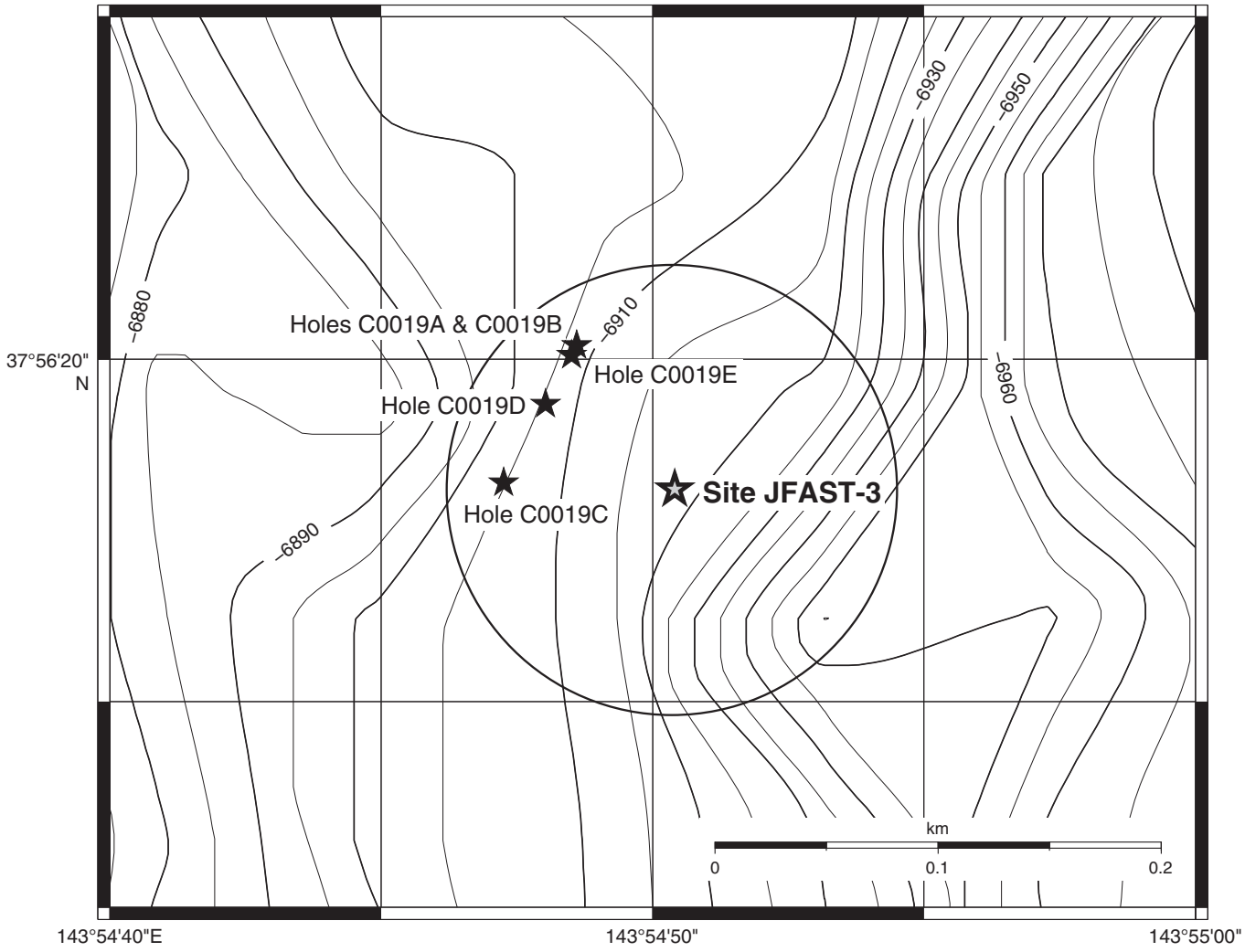

Figure F4. Graphical summary of completed operations at each hole during Expedition 343/343T, showing main logging units and schematic section of total depth for Holes C0019A–C0019E. LWD = logging while drilling. MTL = miniature temperature logger.

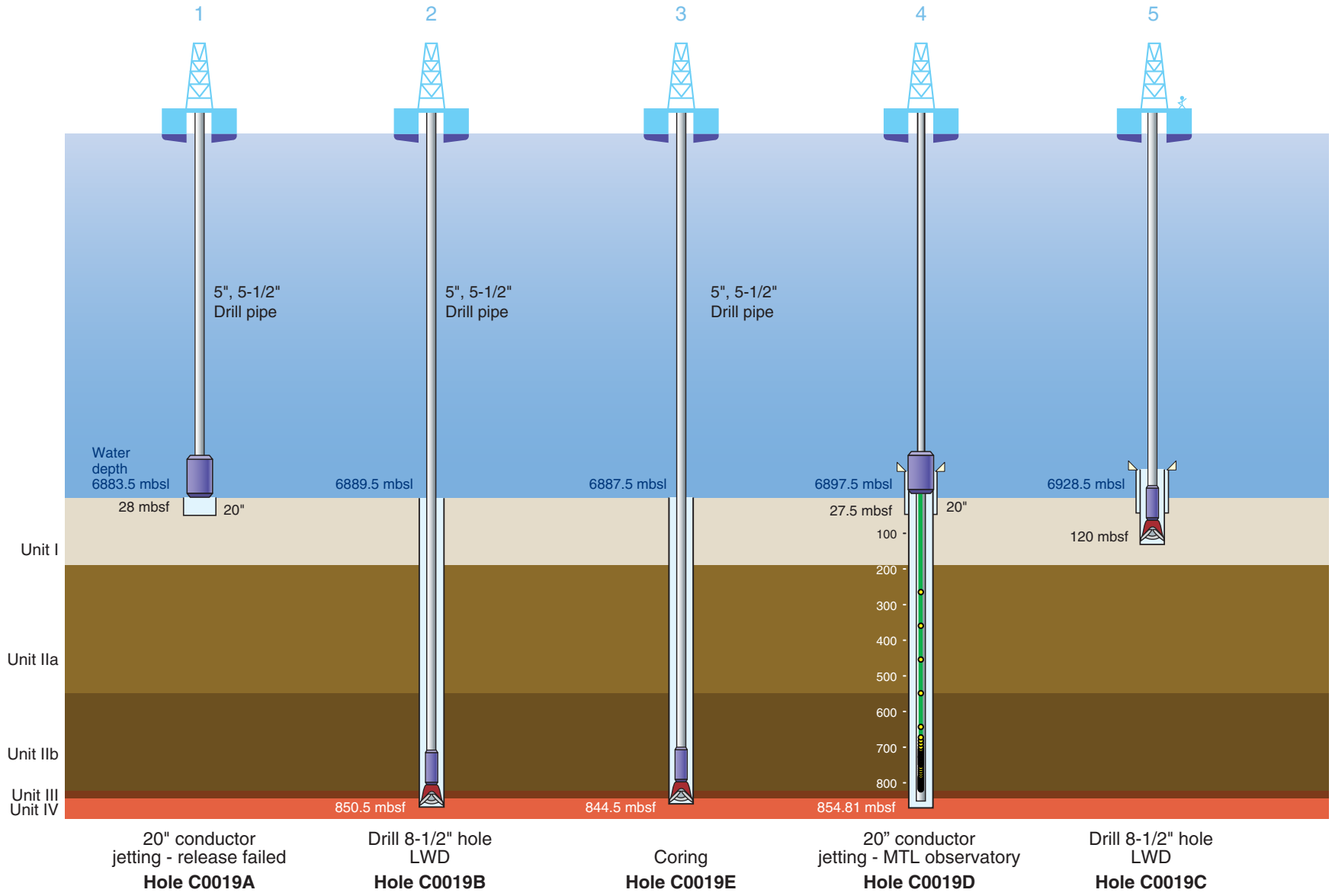

Figure F5. Summary plot of primary geophysical logs as a function of depth, Expedition 343 Hole C0019B. ECAL = electrical caliper, RAB = resistivity-at-the-bit.

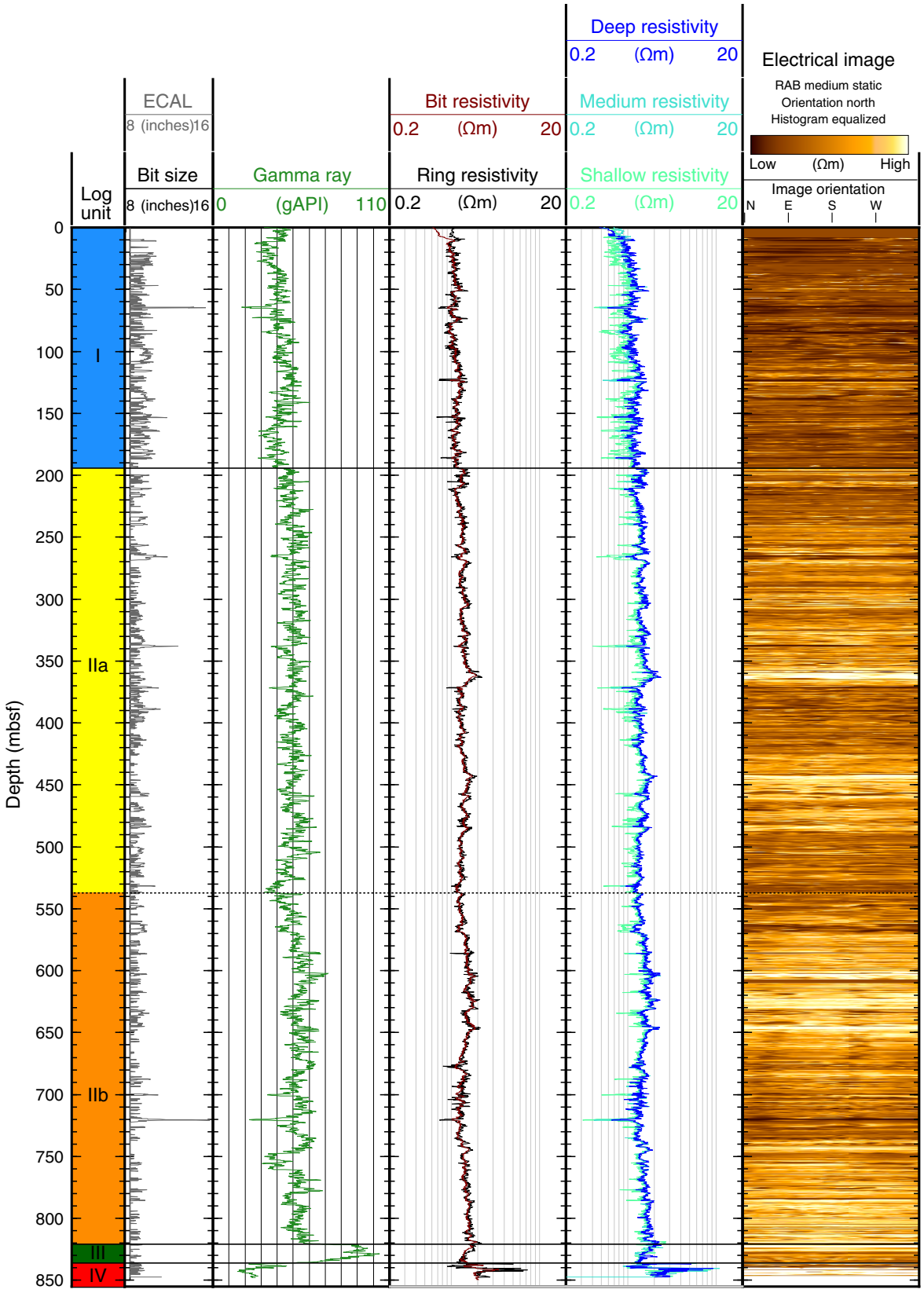

Figure F6. Identification of structural domains in Hole C0019B based on LWD image logs. Bedding and fracture dips identified in image logs are plotted as a function of depth; significant changes in dip distributions constitute the basis for identifying three structural domains. Apparent dips of bedding in the plane of the in-line seismic section through the borehole indicate a predominance of oceanward dipping panels of sediment at intermediate borehole depths, and the structural interpretation illustrates the pronounced disruption of bedding in the vicinity of the 720 and 820 faults. Structural domain f = fault zone.

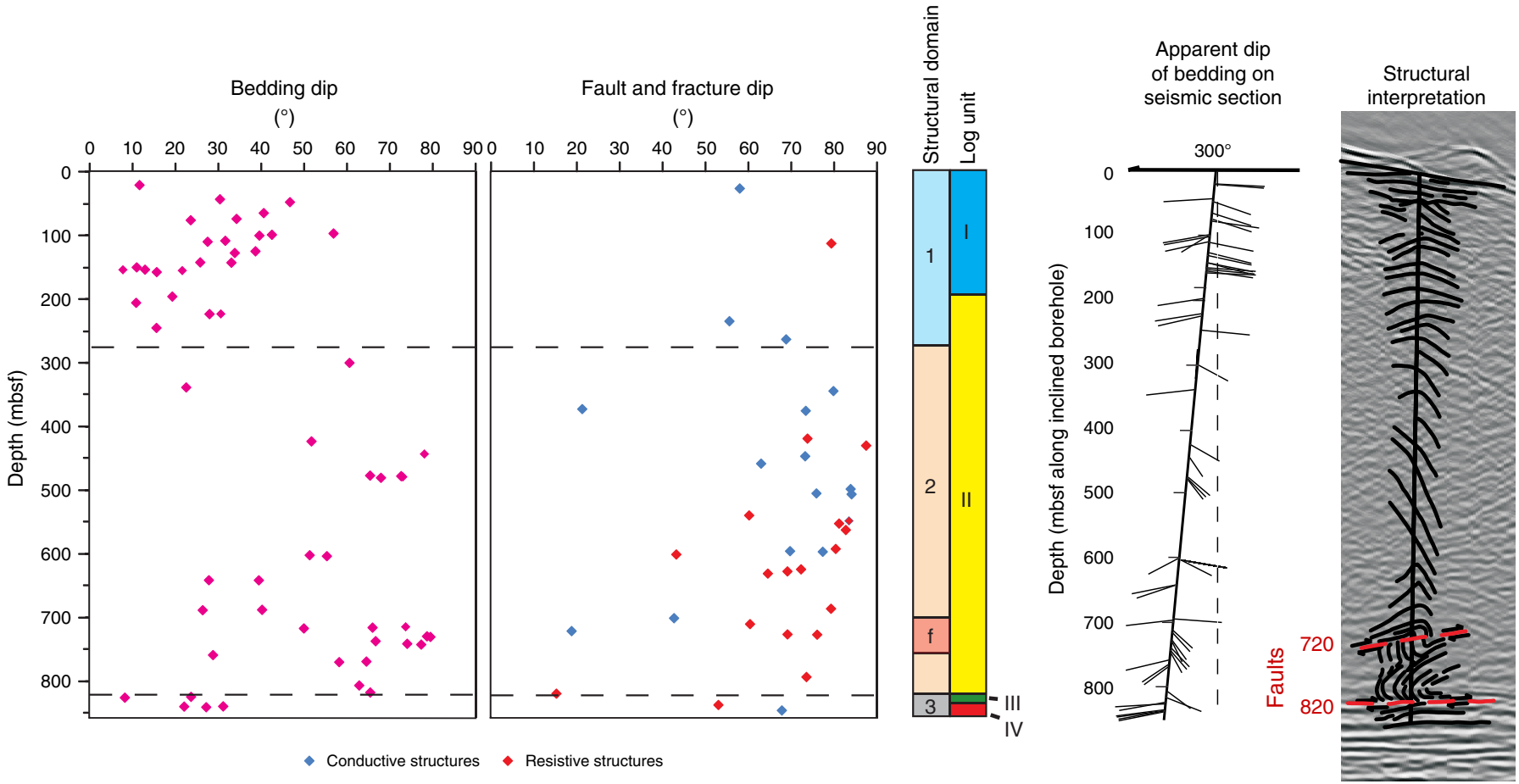

Figure F7. Borehole breakout orientation determined from image logs as a function of depth, Hole C0019B. Breakout azimuths (red circles) are used to identify depth ranges of preferred orientations and general trends in orientations (dashed lines).

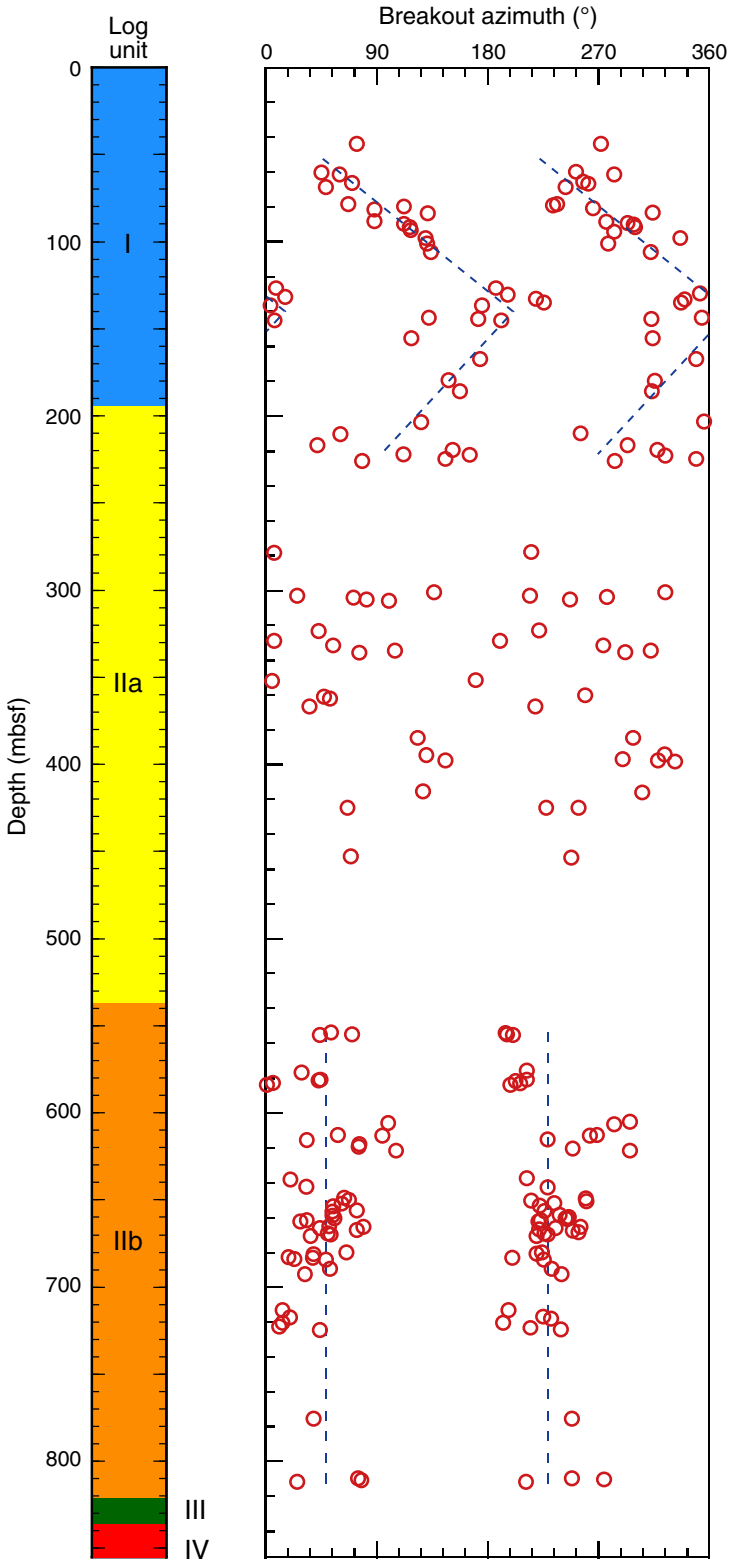

Figure F8. Plot of temperature sensor distribution for the miniature temperature logger (MTL) autonomous observatory deployed in Hole C0019D during Expedition 343T. The density of sensors increased near the 720 and 820 faults in order to accurately define the transient temperature anomaly produced by heating from the Tohoku earthquake. The dense spacing is necessary to resolve the temperature anomaly, which is illustrated for a model temperature distribution in the vicinity of the 820 fault at 1 and 5 y since the earthquake.

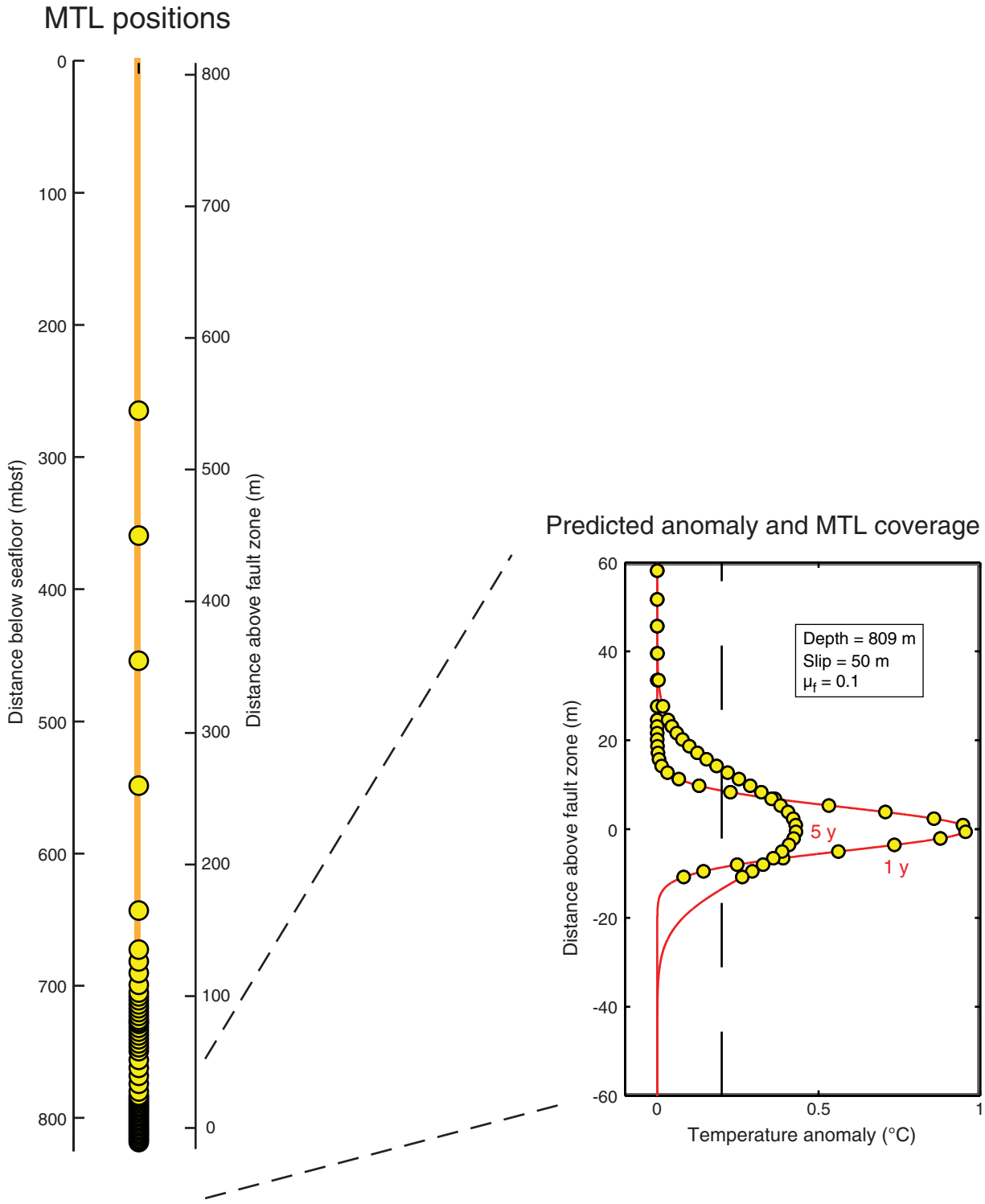

Figure F9. Graphical representation of intervals cored in Expedition 343 Hole C0019E. Time limitations demanded only targeted coring, so the majority of cores were taken from the intervals spanning the 720 and 820 faults. Lithology determined on the basis of visual core description (see text) is represented by color in the lithologic column. VE = vertical exaggeration.

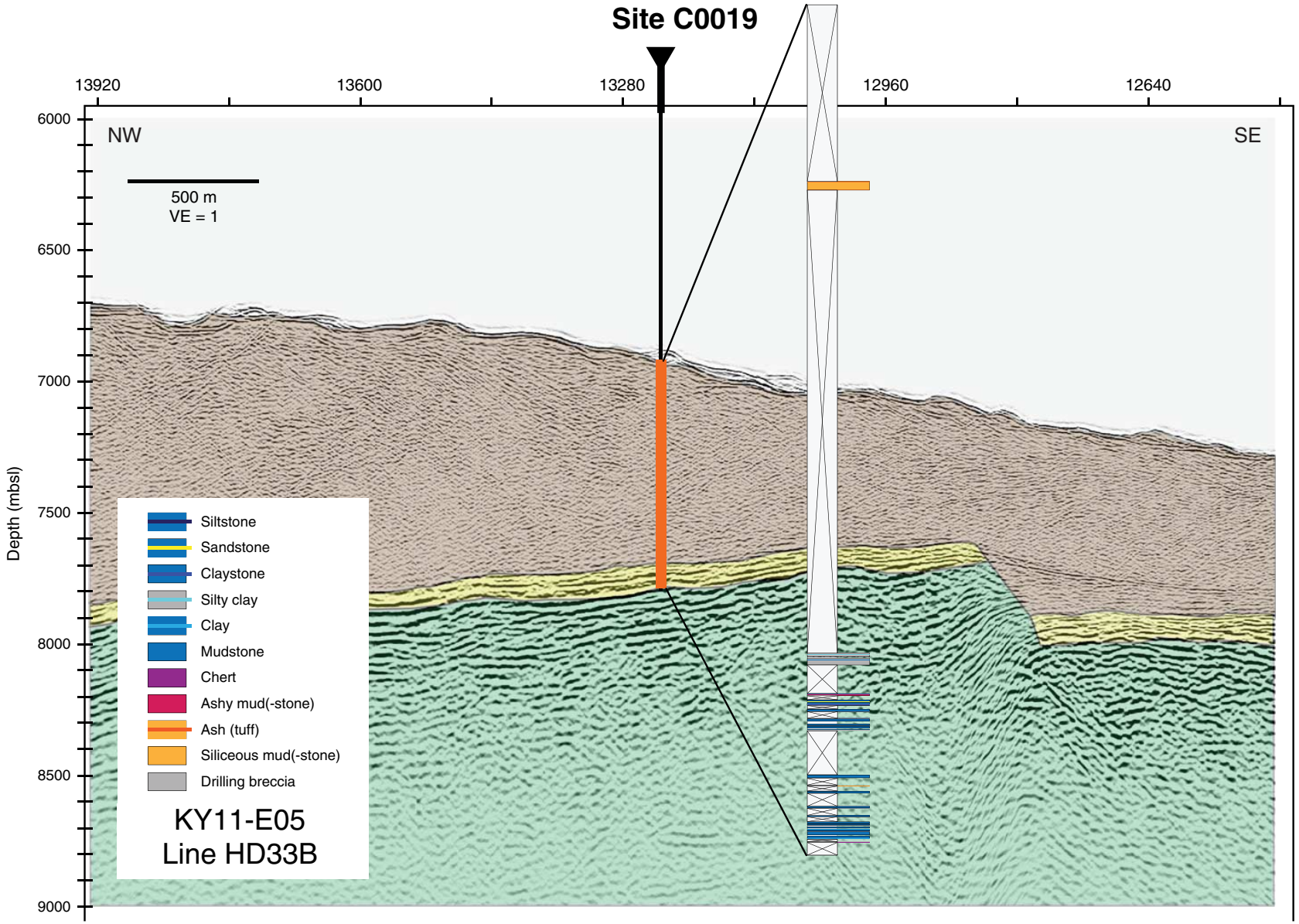

Figure F10. Overview of core-log-seismic integration, showing intervals cored and corresponding measurements of physical properties from discrete samples (circles) and multisensor core logger (MSCL) (line segments) compared to geophysical log data (curves) as a function of depth over the borehole portions where core samples were acquired. Seismic velocity (V_P) calculated from logging data is compared to measurement of velocity; calculated velocity was used to generate synthetic seismic traces to aid in seismic profile interpretation. NGR = natural gamma radiation, NCR = non-contact resistivity, MAD = moisture and density, LWD = logging while drilling, RAB = resistivity-at-the-bit.